Article
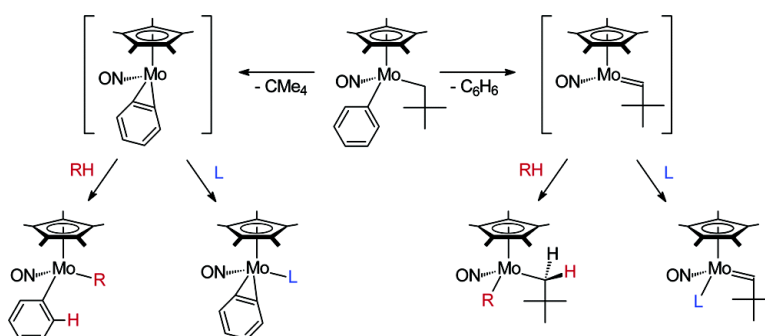
# Intermolecular Activation of Hydrocarbon C–H Bonds under Ambient Conditions by 16-Electron Neopentylidene and Benzyne Complexes of Molybdenum

Kenji Wada, Craig B. Pamplin, Peter Legzdins, Brian O. Patrick, Irina Tsyba, and Robert Bau

## More About This Article

Additional resources and features associated with this article are available within the HTML version:

- Supporting Information
- Links to the 16 articles that cite this article, as of the time of this article download
- Access to high resolution figures
- Links to articles and content related to this article
- Copyright permission to reproduce figures and/or text from this article

View the Full Text HTML

# J|A|C|S

### A R T I C L E S

# Intermolecular Activation of Hydrocarbon C−H Bonds under Ambient Conditions by 16-Electron Neopentylidene and Benzyne Complexes of Molybdenum

Kenji Wada,[†,§] Craig B. Pamplin,[†] Peter Legzdins,*,[†] Brian O. Patrick,[†] Irina Tsyba,[‡] and Robert Bau[‡]

*Contribution from the Departments of Chemistry, University of British Columbia, Vancouver, British Columbia, Canada V6T 1Z1 and University of Southern California, Los Angeles, California 90089*

Received February 27, 2003;  E-mail: legzdins@chem.ubc.ca

***Abstract:*** Cp*Mo(NO)(CH$_2$CMe$_3$)$_2$ (**1**), a complex with $\alpha$-agostic C−H$\cdots$Mo interactions, evolves neopentane in neat hydrocarbon solutions at room temperature and forms the transient 16-electron alkylidene complex, Cp*Mo(NO)(=CHCMe$_3$), which subsequently activates solvent C−H bonds. Thus, it reacts with tetramethylsilane or mesitylene to form Cp*Mo(NO)(CH$_2$CMe$_3$)(CH$_2$SiMe$_3$) (**2**) or Cp*Mo(NO)(CH$_2$CMe$_3$)($\eta^2$-CH$_2$C$_6$H$_3$-3,5-Me$_2$) (**3**), respectively, in nearly quantitative yields. Under identical conditions, **1** in *p*-xylene generates a mixture of sp$^2$ and sp$^3$ C−H bond activation products, namely Cp*Mo(NO)(CH$_2$CMe$_3$)(C$_6$H$_3$-2,5-Me$_2$) (**4**, 73%) and Cp*Mo(NO)(CH$_2$CMe$_3$)($\eta^2$-CH$_2$C$_6$H$_4$-4-Me) (**5**, 27%). In benzene at room temperature, **1** transforms to a mixture of Cp*Mo(NO)(CH$_2$CMe$_3$)(C$_6$H$_5$) (**6**) and Cp*Mo(NO)(C$_6$H$_5$)$_2$ (**7**) in a sequential manner. Most interestingly, the thermal activation of **6** at ambient temperatures gives rise to two parallel modes of reactivity involving either the elimination of benzene and formation of Cp*Mo(NO)(=CHCMe$_3$) or the elimination of neopentane and formation of the benzyne complex, Cp*Mo(NO)($\eta^2$-C$_6$H$_4$). In pyridine, these intermediates are trapped as the isolable 18-electron adducts, Cp*Mo(NO)(=CHCMe$_3$)(NC$_5$H$_5$) (**8**) and Cp*Mo(NO)($\eta^2$-C$_6$H$_4$)(NC$_5$H$_5$) (**9**), and, in hydrocarbon solvents, they effect the intermolecular activation of aliphatic C−H bonds at room temperature to generate mixtures of neopentyl- and phenyl-containing derivatives. However, the distribution of products resulting from the hydrocarbon activations is dependent on the nature of the solvent, probably due to solvation effects and the presence of $\sigma$- or $\pi$-hydrocarbon complexes on the reaction coordinates of the alkylidene and the benzyne intermediates. The results of DFT calculations on these processes in the gas phase support the existence of such hydrocarbon complexes and indicate that better agreement with experimental observations is obtained when the actual neopentyl ligand rather than the simpler methyl ligand is used in the model complexes.

## Introduction

Considerable effort is currently being devoted to the study of selective, intermolecular C−H bond-activation processes with a view to developing efficient and catalytic methods for the direct conversion of hydrocarbon feedstocks into functionalized organic compounds.[1] To date, advances in this field have included the discoveries of various types of metal-containing complexes that effect selective C−H bond activations. Notable examples are late-transition-metal complexes that oxidatively add C−H bonds to the metal center, transition-metal, lanthanide, and actinide complexes that facilitate C−H activation via M−C $\sigma$-bond metathesis and early- to mid-transition-metal complexes that add substrate C−H bonds across M=NR or M=CHR linkages.[1]

Our contribution to this area of chemistry derives from our abiding interest in the family of Cp′M(NO)R$_2$ complexes (Cp′ = Cp ($\eta^5$-C$_5$H$_5$) or Cp* ($\eta^5$-C$_5$Me$_5$); M = Mo or W; R = alkyl or aryl) due to their unique thermal behavior in hydrocarbon solutions. Previous reports from our laboratories have described the thermal conversion of Cp*W(NO)(hydrocarbyl)$_2$ complexes into transient tungsten alkylidene,[2,3] acetylene,[4] or allene[5] species that subsequently activate the C−H bonds of hydrocarbon solvents, often in an unprecedented manner. The reactive

† University of British Columbia.
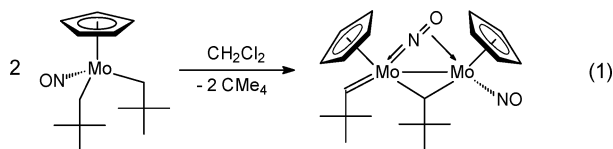‡ University of Southern California.
§ Current address: Department of Energy & Hydrocarbon Chemistry, Graduate School of Engineering, Kyoto University, Sakyo-ku, Kyoto 606-8501, Japan.

(1) Labinger, J. A.; Bercaw, J. E. *Nature* **2002**, *417*, 507−514 and references therein.

(2) (a) Tran, E.; Legzdins, P. *J. Am. Chem. Soc.* **1997**, *119*, 5071−5072. (b) Adams, C. S.; Legzdins, P.; Tran, E. *J. Am. Chem. Soc.* **2001**, *123*, 612−624.

(3) For three other reported examples of intermolecular C−H activations by alkylidene complexes, see: (a) Coles, M. P.; Gibson, V. C.; Clegg, W.; Elsegood, M. R. J.; Porelli, P. A. *J. Chem. Soc., Chem. Commun.* **1996**, 1963−1964. (b) van der Heijden, H.; Hessen, B. *J. Chem. Soc., Chem. Commun.* **1995**, 145−146. (c) Cheon, J.; Rogers, D. M.; Girolami, G. S. *J. Am. Chem. Soc.* **1997**, *119*, 6804−6813.

(4) (a) Debad, J. D.; Legzdins, P.; Lumb, S. A.; Batchelor, R. J.; Einstein, F. W. B. *J. Am. Chem. Soc.* **1995**, *117*, 3288−3289. (b) Legzdins, P.; Lumb, S. A. *Organometallics* **1997**, *16*, 1825−1827. (c) Debad, D.; Legzdins, P.; Lumb, S. A.; Rettig, S. J.; Batchelor, R. J.; Einstein, F. W. B. *Organometallics* **1999**, *18*, 3414−3428.

(5) Ng, S. H. K.; Adams, C. S.; Legzdins, P. *J. Am. Chem. Soc.* **2002**, *124*, 9380−9381.

**Table 1.** X-ray Crystallographic Data for Complexes **1**, **3**, **6**, **8**, and **9**·$C_6H_6$

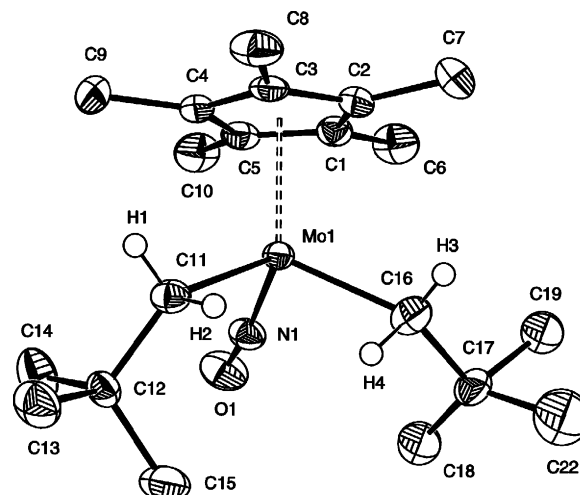| | 1 | 3 | 6 | 8 | 9·$C_6H_6$ |
|---|---|---|---|---|---|
| empirical formula | $C_{20}H_{37}MoNO$ | $C_{24}H_{37}MoNO$ | $C_{21}H_{31}MoNO$ | $C_{20}H_{30}MoN_2O$ | $C_{27}H_{30}MoN_2O$ |
| formula weight | 403.45 | 451.49 | 409.41 | 410.40 | 494.47 |
| crystal size (mm³) | $0.37 \times 0.24 \times 0.015$ | $0.20 \times 0.20 \times 0.20$ | $0.30 \times 0.20 \times 0.20$ | $0.57 \times 0.22 \times 0.18$ | $0.20 \times 0.05 \times 0.05$ |
| crystal system | monoclinic | monoclinic | monoclinic | triclinic | orthorhombic |
| space group | $P2_1/n$ | $P2_1/n$ | $P2_1/c$ | $P\bar{1}$ | $P2_12_12_1$ |
| volume (Å³) | 2097.4(7) | 2305.4(3) | 2061.86(17) | 1015.4(9) | 2300.8(2) |
| $a$ (Å) | 8.9121(17) | 13.1900(11) | 10.2911(5) | 8.372(4) | 7.8177(4) |
| $b$ (Å) | 21.702(4) | 11.8175(7) | 14.6191(6) | 8.944(5) | 14.3141(9) |
| $c$ (Å) | 11.260(2) | 15.1108(13) | 14.4274(8) | 14.795(8) | 20.5603(10) |
| $\alpha$ (deg) | 90 | 90 | 90 | 81.399(9) | 90 |
| $\beta$ (deg) | 105.610(3) | 101.828(4) | 108.209(2) | 79.463(8) | 90 |
| $\gamma$ (deg) | 90 | 90 | 90 | 69.442(8) | 90 |
| $Z$ | 4 | 4 | 4 | 2 | 4 |
| density (g cm⁻³) | 1.278 | 1.301 | 1.319 | 1.342 | 1.428 |
| wavelength (Å) | 0.710 73 | 0.710 73 | 0.710 69 | 0.710 73 | 0.710 73 |
| temp (K) | 130(2) | 173(2) | 173(2) | 160(2) | 173(2) |
| $\mu$ (cm⁻¹) | 6.30 | 5.81 | 6.43 | 6.54 | 5.91 |
| $F_{000}$ | 856 | 952 | 856 | 428 | 1024 |
| $R_1$ | 0.0444 | 0.0413 | 0.0285 | 0.0473 | 0.0327 |
| $wR_2$ | 0.1038 | 0.1018 | 0.0780 | 0.1230 | 0.0662 |

tungsten species are typically formed by thermolysis of appropriate organometallic precursors at temperatures ranging from 50 to 80 °C. However, under these conditions some of the C−H activation processes lead to cascade-type or decomposition processes, and the operative chemistry is often obscured by the thermal instability of the organometallic complexes involved. Consequently, we decided to extend our studies to encompass the congeneric molybdenum precursors in hopes of overcoming this difficulty. We began our investigations in this regard with Cp*Mo(NO)(CH₂CMe₃)₂ (**1**), since we knew from our previous work that the related CpMo(NO)(CH₂CMe₃)₂ complex in CH₂-Cl₂ eliminates neopentane below room temperature and forms the bimetallic complex [CpMo(NO)][μ-η¹:η²-NO)(μ-CHCMe₃)-[CpMo=CHCMe₃] via a transient alkylidene species (eq 1).[6]

$$2 \quad \underset{ON^{\backslash\backslash}}{\overset{}{Mo}} \quad \xrightarrow[- \, 2 \, CMe_4]{CH_2Cl_2} \quad \text{complex structure} \qquad (1)$$

In this report, we present the results of our investigations of the thermal chemistry of **1** in various solvents, a survey that has revealed both similarities and differences with that established for its well-studied tungsten analogue. We also describe the results of DFT calculations on some of these processes in the gas phase that provide additional insight as to the mechanistic pathways being followed during these metal-mediated transformations. A portion of this work has been communicated previously.[7]

## Results and Discussion

**Solid-State and Solution Molecular Structures of Cp*Mo-(NO)(CH₂CMe₃)₂ (1).** As might have been expected, the molecular structures of **1** in both the solid state and solutions are virtually identical to those of its tungsten congener.[8] Both

(6) (a) Legzdins, P.; Rettig, S. J.; Veltheer, J. E. *J. Am. Chem. Soc.* **1992**, *114*, 6922−6923. (b) Legzdins, P.; Rettig, S. J.; Veltheer, J. E.; Batchelor, R. J.; Einstein, F. W. B. *Organometallics* **1993**, *12*, 3575−3585.
(7) Wada, K.; Pamplin, C. B.; Legzdins, P. *J. Am. Chem. Soc.* **2002**, *124*, 9680−9681.
(8) Bau, R.; Mason, S. A.; Patrick, B. O.; Adams, C. S.; Sharp, W. B.; Legzdins, P. *Organometallics* **2001**, *20*, 4492−4501.

**Figure 1.** ORTEP plot of the solid-state molecular structure of Cp*Mo-(NO)(CH₂CMe₃)₂ (**1**) with 50% probability ellipsoids. Selected bond lengths (Å) and angles (deg): Mo(1)−N(1) = 1.757(3), N(1)−O(1) = 1.216(4), Mo(1)−C(11) = 2.163(3), Mo(1)−C(16) = 2.098(4), Mo(1)−H(4) = 2.18-(6), Mo(1)−N(1)−O(1) = 168.5(3), N(1)−Mo(1)−C(11) = 98.73(13), N(1)−Mo(1)−C(16) = 98.55(15), and C(11)−Mo(1)−C(16) = 108.77-(15).

Cp*M(NO)(CH₂CMe₃)₂ (M = Mo, W) molecular complexes are isomorphous and crystallize in the $P2_1/n$ space group with essentially the same unit-cell dimensions (Table 1). A single-crystal X-ray diffraction analysis of **1** at 130(2) K has confirmed its monomeric nature and has provided the ORTEP diagram and intramolecular metrical parameters presented in Figure 1. The Cp*−Mo and Mo−NO intramolecular dimensions are similar to those found in related complexes.[9] There is some rotational disorder in the methyl groups of one neopentyl ligand; however, this disorder has no effect on the positions of the atoms of its methylene group. One of the methylene C−H bonds, C(16)−H(4), is strongly distorted toward the Mo atom in an orientation consistent with interaction between this C−H bond and the vacant metal-based d orbital. The Mo(1)−C(16)−H(4) angle associated with this bond (81(3)°) is much lower than the normal value (109.5°) expected for an sp³-hybridized C atom, and the Mo(1)···H(4) distance of 2.18(6) Å is in the range

(9) Legzdins, P.; Veltheer, J. E. *Acc. Chem. Res.* **1993**, *26*, 41−48.

anticipated for an agostic interaction. In addition to this agostic C−H···Mo interaction, another methylene hydrogen, H(2), appears to be interacting very weakly with the Mo atom, but this interaction is much more subtle [C(11)−H(2) = 0.97(4) Å; Mo(1)−C(11)−H(2) = 99(2)°]. Nevertheless, the structural deformations ascribed to agostic interactions in **1** are very similar to those revealed in its tungsten congener by a low-temperature X-ray analysis. This "unequal double α-agostic" motif has been more definitively established for the tungsten complex by a neutron diffraction analysis at 120 K.[8]
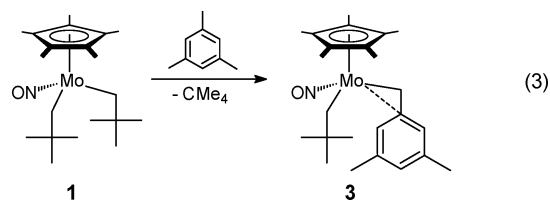
The $^1H$ and gated-decoupled $^{13}C$ NMR spectra of **1** in toluene-$d_8$ at 0 °C indicate that the α-agostic interactions evident in the solid-state structure persist in solutions. First, there is a large chemical-shift difference ($\Delta\delta = 4.02$) between the methylene proton signals that appear as doublets in the $^1H$ NMR spectrum with one doublet appearing at $\delta = -1.06$ ppm. Second, there are unequal $^1J_{CH}$ values ($\Delta^1J_{CH} = 24$ Hz) evident for the α-carbon signals in the gated-decoupled $^{13}C$ NMR spectrum with one being significantly reduced (i.e., $^1J_{CH} = 101$ Hz) when compared to normal values. Indeed, both NMR spectra of **1** closely resemble those exhibited by $Cp^*W(NO)(CH_2CMe_3)_2$ (e.g., for the W compound, $\Delta^1J_{CH} = 23$ Hz).[8] In summary, there is essentially no difference between the molecular structures of the Mo and W complexes either in the solid state or in solutions. Both isostructural complexes are appropriately configured to undergo cleavage of an α-H bond by a metal-assisted abstraction process, and hence, there is no apparent structural basis for the experimentally observed differences in thermal sensitivity of the Mo and W compounds (vide infra).

**Thermal C−H Bond-Activation Chemistry Initiated by $Cp^*Mo(NO)(CH_2CMe_3)_2$ (1). A. Activation of Tetramethylsilane.** Stirred solutions of **1** in tetramethylsilane at room temperature evolve neopentane over 28 h as the known[10] mixed alkyl complex, $Cp^*Mo(NO)(CH_2CMe_3)(CH_2SiMe_3)$ (**2**), is formed in quantitative yield (eq 2). Complex **2** is formed from

(2)
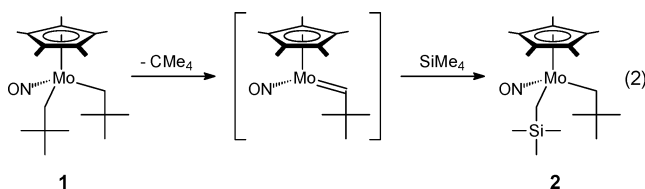
**1** via the activation of an sp³ C−H bond of a solvent molecule, and it does not react further with tetramethylsilane under these mild reaction conditions. In contrast, the analogous tungsten complex reacts with tetramethylsilane under the requisite thermolysis conditions (70 °C, 40 h) to generate a mixture of $Cp^*W(NO)(CH_2CMe_3)(CH_2SiMe_3)$ (97%) and $Cp^*W(NO)(CH_2SiMe_3)_2$ (3%).[2] The second product presumably results from the elimination of neopentane from $Cp^*W(NO)(CH_2CMe_3)(CH_2SiMe_3)$ and formation of transient $Cp^*W(NO)(=CHSiMe_3)$ that subsequently activates a second solvent molecule.

**B. Activation of Mesitylene.** The thermal reaction of **1** in neat mesitylene affords $Cp^*Mo(NO)(CH_2CMe_3)(\eta^2-CH_2C_6H_3-3,5-Me_2)$ (**3**) in ca. 95% yield after 28 h at room temperature (eq 3). No signals attributable to any other C−H bond-activation products are evident in the $^1H$ NMR spectrum of the final reaction mixture. Complex **3** exhibits $^1H$ and $^{13}C\{^1H\}$ NMR

(10) Debad, J. D.; Legzdins, P.; Rettig, S. J.; Veltheer, J. E. *Organometallics* **1993**, *12*, 2714−2725.

(3)

spectra that indicate that the bulky 3,5-dimethylbenzyl ligand is attached to the metal in an $\eta^2$ fashion on average in solution.[11] The existence of this coordination mode is indicated by a broad $^1H$ NMR resonance at $\delta$ 5.94 that can be attributed to the ortho H atoms of this ligand and the occurrence of a high-field ipso carbon resonance at $\delta$ 118.4 in the $^{13}C\{^1H\}$ spectrum. Our inference of this mode of attachment is further supported by the solid-state molecular structure of **3** (Figure 2) that clearly shows an $\eta^2$-3,5-dimethylbenzyl ligand having a bonding contact between the ipso carbon and the metal center (Mo(1)−C(12) = 2.496(3) Å) and an acute Mo−C−C$_{ipso}$ bond angle of 84.0-(2)°. The other metrical parameters associated with the $\eta^2$-3,5-dimethylbenzyl ligand of **3** are similar to those extant in $Cp^*Mo(NO)(CH_2SiMe_3)(\eta^2-CH_2C_6H_5)$ and related benzyl complexes.[12] The propensity of benzyl ligands to exhibit $\eta^2$ coordination modes in such complexes has been attributed to their ability to provide in this manner the necessary extra electron density to impart an 18e configuration to the metal center.

**C. Activation of *p*-Xylene.** The reaction of **1** in *p*-xylene at room temperature generates products derived from the activation of solvent sp² and sp³ C−H bonds. Specifically, the aryl complex $Cp^*Mo(NO)(CH_2CMe_3)(C_6H_3-2,5-Me_2)$ (**4**, 73%) and the known[12b] 4-methylbenzyl complex $Cp^*Mo(NO)(CH_2CMe_3)-(\eta^2-CH_2C_6H_4-4-Me)$ (**5**, 27%) are formed (eq 4). Although

(4)
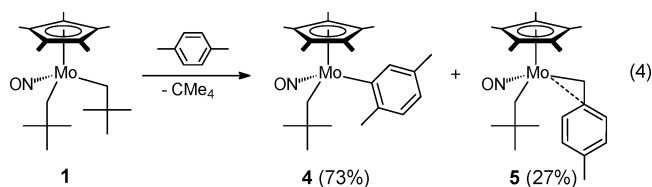
isomeric complexes **4** and **5** have not been isolated in pure form from the final reaction mixture, they have been identified on the basis of NMR spectroscopic, mass spectral, and elemental analysis data. The NMR spectral features of **4** are consistent with the formation of a single isomer with the structure shown in eq 4, unlike the related tungsten complex $Cp^*W(NO)(CH_2-CMe_3)(C_6H_3-2,5-Me_2)$, which exists as two rapidly interchanging isomers in solution at room temperature.[13] The solution $^1H$ NMR spectrum of **5**, like that of the related complex **3**, reveals the presence of an $\eta^2$-4-methylbenzyl ligand and exhibits four sets of resonances due to the diastereotopic methylene H atoms.

**D. Activation of Benzene-$d_6$ and Mechanistic Considerations.** Complex **1** in $C_6D_6$ is converted to $Cp^*Mo(NO)-(CHDCMe_3)(C_6D_5)$ (**6**-$d_6$) over the course of 28 h at room temperature (eq 5). The 1,2-C−D bond addition of $C_6D_6$ across
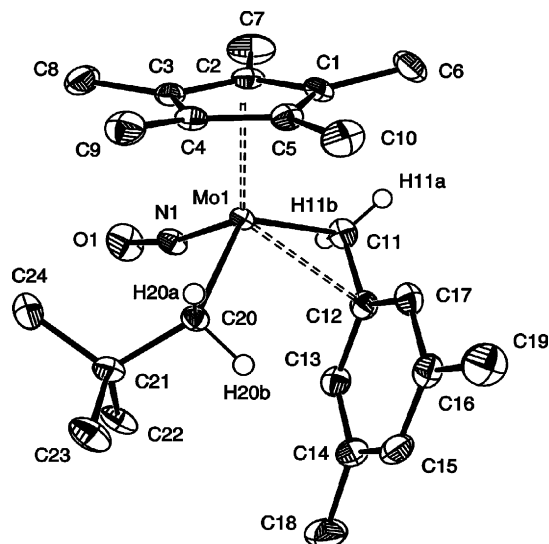
(11) Legzdins, P.; Jones, R. H.; Phillips, E. C.; Yee, V. C.; Trotter, J.; Einstein, F. W. B. *Organometallics* **1991**, *10*, 986−1002.
(12) (a) Dryden, N. H.; Legzdins, P.; Phillips, E. C.; Trotter, J.; Yee, V. C. *Organometallics* **1990**, *9*, 882−884. (b) Dryden, N. H.; Legzdins, P.; Trotter, J.; Yee, V. C. *Organometallics* **1991**, *10*, 2857−2870.
(13) Adams, C. S.; Legzdins, P.; Tran, E. *Organometallics* **2002**, *21*, 1474−1486.

**Figure 2.** ORTEP plot of the solid-state molecular structure of Cp*Mo-(NO)(CH₂CMe₃)($\eta^2$-CH₂C₆H₃-3,5-Me₂) (**3**) with 50% probability ellipsoids. Selected bond lengths (Å) and angles (deg): $Mo(1)-N(1) = 1.761(2)$, $N(1)-O(1) = 1.226(3)$, $Mo(1)-C(11) = 2.189(3)$, $Mo(1)-C(12) = 2.496$-(3), $Mo(1)-C(20) = 2.226(3)$, $C(11)-C(12) = 1.450(4)$, $Mo(1)-N(1)-O(1) = 168.1(2)$, $Mo(1)-C(11)-C(12) = 84.00(19)$, and $C(11)-Mo(1)-C(12) = 35.28(11)$.

the Mo=C bond of the intermediate alkylidene complex is stereospecific, with incorporation of deuterium at the synclinal methylene position being indicated by the absence of a corresponding resonance in the ¹H NMR spectrum of **6**-$d_6$. Furthermore, the anticlinal methylene-proton signal appears as a broad singlet due to an unresolved coupling to the geminal deuterium nucleus. These features are similar to the spectral characteristics noted previously for the related tungsten complex, which is formed in a similar manner but at higher temperatures.[2b]
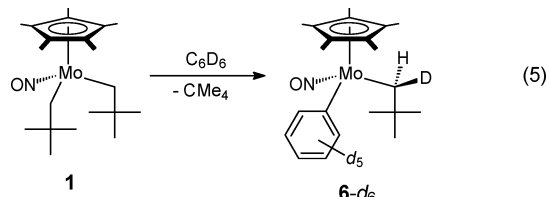


Kinetic studies of α-hydrogen elimination from **1** have been carried out in C₆D₆ solution by monitoring the decay of the Cp* resonance of **1** using ¹H NMR spectroscopy in the temperature range 26−40 °C. The onset of neopentane elimination from **1** is indicated by a growth in the resonances due to **6**-$d_6$ and neopentane (δ 0.90). The activation parameters $\Delta H^\ddagger = 99(1)$ kJ mol⁻¹ and $\Delta S^\ddagger = -11(4)$ J mol⁻¹ K⁻¹ for this transformation can be determined using regression methods from a linear plot of $\ln(k/T)$ versus $1/T$, and they are consistent with the rate-determining step being the elimination of neopentane from **1**. In addition, the thermolysis of **1** in a 1:1 mixture of benzene/benzene-$d_6$ at 23 °C yields an intermolecular KIE of 1.04(4), a value similar to that exhibited by its tungsten congener at 70 °C. In other words, all current indications are that the Cp*M(NO)(CH₂CMe₃)₂ (M = Mo, W) complexes follow very similar mechanistic pathways during their thermal activations of hydrocarbon C−H bonds.

**E. Activation of Benzene.** Remarkably, the reaction of **1** with C₆H₆ at room temperature results in the sequential activation

**Scheme 1**
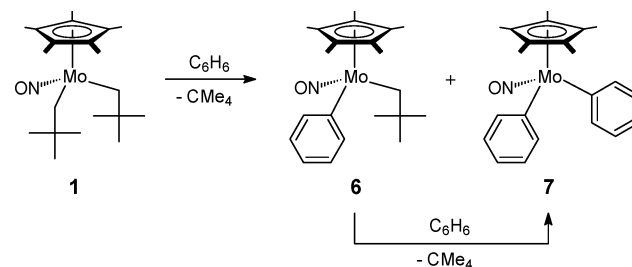


of two molecules of benzene and the formation of the two complexes Cp*Mo(NO)(CH₂CMe₃)(C₆H₅) (**6**) and Cp*Mo(NO)-(C₆H₅)₂ (**7**) in the final reaction mixture (Scheme 1). As shown in Scheme 1, the reaction of **6** with C₆H₆ at room temperature also cleanly generates **7**. The yield of **6** can therefore be maximized by workup of the crude reaction mixture upon complete consumption of **1**, that is, after ca. 28 h at room temperature. Complex **6** can be purified by extraction from the crude residue into cold pentane followed by column chromatography on alumina, and it is isolable as a red crystalline solid (27% yield).
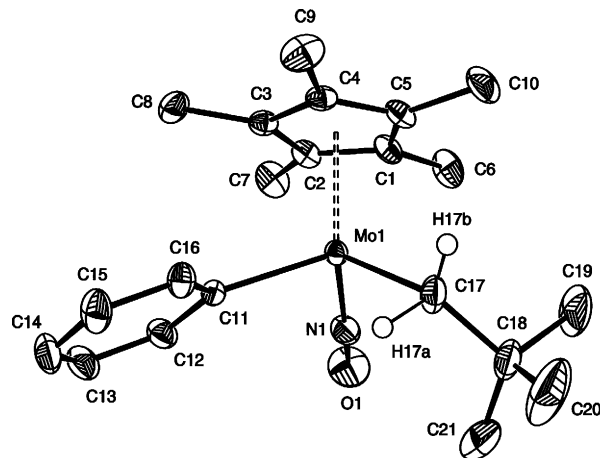


**Figure 3.** ORTEP plot of the solid-state molecular structure of Cp*Mo-(NO)(CH₂CMe₃)(C₆H₅) (**6**) with 50% probability ellipsoids. Selected bond lengths (Å) and angles (deg): $Mo(1)-N(1) = 1.769(2)$, $N(1)-O(1) = 1.214$-(2), $Mo(1)-C(11) = 2.148(2)$, $Mo(1)-C(17) = 2.091(2)$, $Mo(1)-H(17a) = 2.13(3)$, $Mo(1)-H(17b) = 2.57(3)$, $C(17)-C(18) = 1.530(3)$, $Mo(1)-N(1)-O(1) = 167.5(2)$, $Mo(1)-C(17)-H(17a) = 78(2)$, $Mo(1)-C(17)-H(17b) = 110(2)$, $N(1)-Mo(1)-C(11) = 94.13(8)$, $N(1)-Mo(1)-C(17) = 99.4(1)$, and $C(11)-Mo(1)-C(17) = 113.98(8)$.

The solid-state molecular structure of **6** has been established by a single-crystal X-ray crystallographic analysis. The resulting ORTEP diagram of the three-legged piano-stool structure is shown in Figure 3, and pertinent crystal and refinement data are collected in Table 1. The most notable feature of the structure is the presence of one very strong methylene C−H···Mo agostic interaction ($Mo(1)-H(17a) = 2.13(3)$ Å, $Mo(1)-C(17)-H(17a) = 78(2)°$) that persists in solutions of the complex. The other intramolecular metrical parameters of this molecule resemble those reported for related complexes. In general, aryl complexes of this type, that is, Cp′M(NO)(aryl)(R) (Cp′ = Cp, Cp*; M = Mo, W; R = alkyl, aryl), are known to be thermally sensitive.[2b,14−16]

(14) Dryden, N. H.; Legzdins, P.; Rettig, S. J.; Veltheer, J. E. *Organometallics* **1992**, *11*, 2583−2590.
(15) Sharp, W. B., Ph.D. Dissertation, The University of British Columbia, 2001.
(16) Debad, J. D., Ph.D. Dissertation, The University of British Columbia, 1994.

The pentane-insoluble residue formed from solutions of **1** in benzene consists primarily of the diphenyl complex **7**, which can be isolated in moderate yield (30%) as violet needles by recrystallization from ether. Alternatively, **7** can be prepared in higher yields simply by stirring benzene solutions of **1** (or **6**) at room temperature for extended periods of time. Thus, it is formed virtually quantitatively in a benzene solution of **1** after ca. 1 week at ambient temperatures. Complex **7** in $C_6D_6$ solutions is converted to **7**-$d_6$ at room temperature, and **7**-$d_{10}$ is the only identifiable organometallic complex detected by ^{1}H NMR spectroscopy after 48 h at 40 °C, although higher reaction temperatures also result in the formation of several unidentified decomposition products. The intermediacy of a transient benzyne complex in this chemistry is indicated by the fact that monitoring of the conversion of **6**-$d_6$ to **7**-$d_{10}$ in $C_6D_6$ by ^{2}H{^{1}H} NMR spectroscopy shows no incorporation of deuterium into the Cp* methyl substituents. Hence, mechanisms involving the intramolecular oxidative addition of a Cp* C−H bond to a metal center and formation of intermediate "tuck-in" complexes that are known to result in such deuterium scrambling[17−21] can be ruled out for this chemistry. Another possible mechanism for the C−H bond activation of benzene by **6** involves intermolecular oxidative addition to form a high-valent species such as Cp*Mo-(NO)(H)(C_6H_5)_2(CH_2CMe_3). However, since there is no intermolecular kinetic isotope effect evident during the initial rates of the reaction of **6** with benzene/benzene-$d_6$, this pathway is deemed to be unlikely.

The sequential activation of two molecules of benzene by **1** differs from the otherwise similar chemistry observed previously for the related tungsten complex Cp*W(NO)(CH_2CMe_3)_2, which is converted cleanly to the phenyl complex, Cp*W(NO)(CH_2-CMe_3)(C_6H_5), upon thermolysis in benzene at 70 °C. Cp*W-(NO)(C_6H_5)_2 is not present in the final reaction mixture. In this connection, it may be noted that Cp*W(NO)(CH_2CMe_3)(C_6H_5) converts at 110 °C in benzene solutions containing PMe_3 to Cp*W(NO)(C_6H_5)_2(PMe_3), presumably via a transient benzyne complex.[16] Another difference between the molybdenum and tungsten systems is that Cp*W(NO)(C_6H_5)_2 may be synthesized by treating Cp*W(NO)Cl_2 with 1 equiv of (C_6H_5)_2Mg·$x$(dioxane), but analytically pure samples of Cp*Mo(NO)(C_6H_5)_2 (**7**) are only accessible via the C−H activation of benzene. Previous attempts to prepare **7** by metathetical means provided samples contaminated with MgCl_2, possibly due to the formation of adducts in which the Lewis-basic nitrosyl ligand of **7** acts as a donor to the Lewis-acidic Mg atom of the magnesium chloride byproduct.[22]

To put these observations in context, it may be noted that Girolami and co-workers have shown that thermolysis of the titanium tetrakis(neopentyl) complex, Ti(CH_2CMe_3)_4, in benzene results in the formation of Ti(CH_2CMe_3)_3(C_6H_5).[3c] Deuterium-labeling studies in $C_6D_6$ indicate that this reaction proceeds via distinct alkylidene and titanacyclobutane intermediates formed via α- or γ-hydrogen elimination of neopentane from Ti(CH_2-
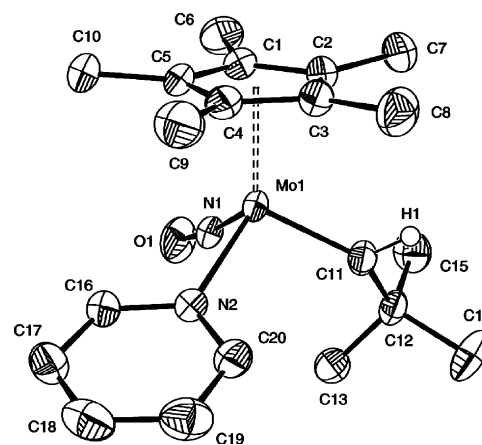


**Figure 4.** ORTEP plot of the solid-state molecular structure of Cp*Mo-(NO)(=CHCMe_3)(NC_5H_5) (**8**) with 50% probability ellipsoids. Selected bond lengths (Å) and angles (deg): Mo(1)−C(11) = 1.951(3), C(11)−H(11) = 0.97(4), Mo(1)−N(1) = 1.764(3), N(1)−O(1) = 1.231(4), Mo-(1)−N(1)−O(1) = 172.4(3), Mo(1)−C(11)−C(12) = 134.9(2), and C(11)−Mo(1)−N(2) = 101.0(1).

CMe_3)_4. The γ-hydrogen activation pathway is about 25 times slower than the α-hydrogen abstraction process. Interestingly, the Ti(CH_2CMe_3)_3(C_6H_5) product reacts further via elimination of a second equivalent of neopentane to generate an ill-defined benzyne intermediate prior to decomposition.

**F. Trapping of the Intermediates.** Given our previous success in trapping and identifying transient intermediates by carrying out the thermolyses of the precursor bis(alkyl) complexes in Lewis bases that are able to stabilize coordinatively unsaturated tungsten[2] and molybdenum[23,24] complexes, we effected the thermolysis of **1** in neat pyridine under ambient conditions. The intermediacy of a neopentylidene complex in the thermal C−H bond activation reactions of **1** is confirmed by the isolation of the base-stabilized complex Cp*Mo(NO)-(=CHCMe_3)(NC_5H_5) (**8**) in moderate yield (55%) from this reaction (eq 6). Complex **8** crystallizes as orange prisms from



(6)
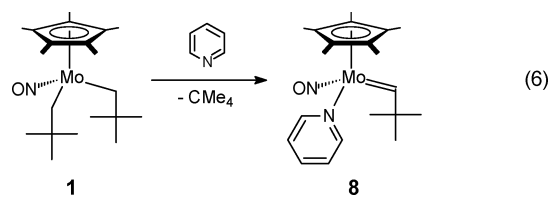
hexanes, and its solid-state molecular structure has been established by a single-crystal X-ray crystallographic analysis. The resulting ORTEP plot is shown in Figure 4. The notable metrical parameters of **8** include a short Mo(1)−C(11) bond distance of 1.951(3) Å and an obtuse Mo−C(11)−C(12) bond angle of 134.9(2)°. The neopentylidene ligand is oriented anticlinal to the Cp* group, thereby minimizing steric interactions and optimizing the synergic π-bonding between the π-donor alkylidene and π-acceptor NO ligands.[25−27] In $C_6D_6$ solution, **8** (which is formed as a single isomer) exhibits typical

(17) Bercaw, J. E. *Adv. Chem. Ser.* **1978**, *167*, 136−148.
(18) Chirik, P. J.; Day, M. W.; Bercaw, J. E. *Organometallics* **1999**, *18*, 1873−1881.
(19) Takao, T.; Amako, M.; Suzuki, H. *Organometallics* **2001**, *20*, 3406−3422.
(20) Kraft, B. M.; Lachicotte, R. J.; Jones, W. D. *J. Am. Chem. Soc.* **2001**, *123*, 10973−10979.
(21) Polse, J. L.; Andersen, R. A.; Bergman, R. G. *J. Am. Chem. Soc.* **1998**, *120*, 13405−13414.
(22) Legzdins, P.; Rettig, S. J.; Sánchez, L. *Organometallics* **1988**, *7*, 2394−2403.
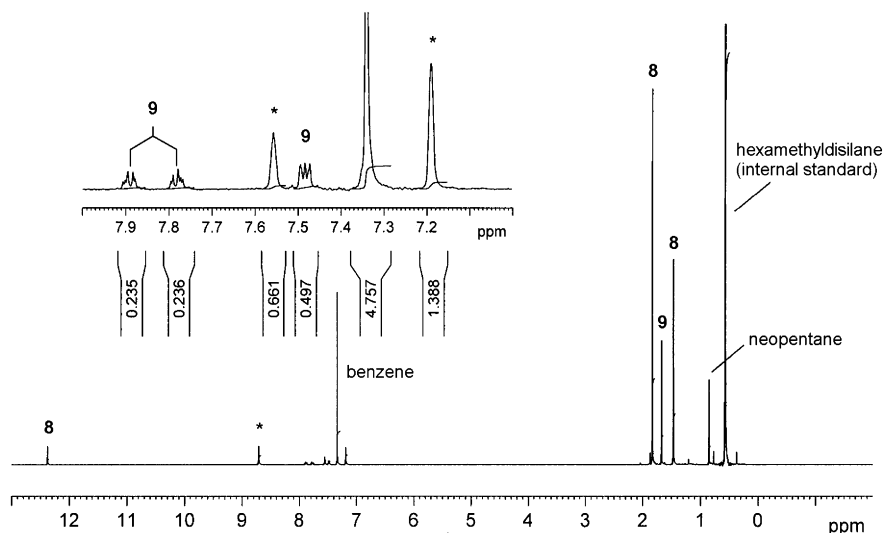
(23) Legzdins, P.; Rettig, S. J.; Veltheer, J. E.; Batchelor, R. J.; Einstein, F. W. B. *Organometallics* **1993**, *12*, 3575−3585.
(24) Legzdins, P.; Veltheer, J. E.; Young, M. A.; Batchelor, R. J.; Einstein, F. W. B. *Organometallics* **1995**, *14*, 407−417.
(25) Schilling, B. E. R.; Hoffman, R.; Faller, J. W. *J. Am. Chem. Soc.* **1979**, *101*, 592−598.
(26) Gibson, V. C. *J. Chem. Soc., Dalton Trans.* **1994**, 1607−1618.
(27) Smith, K. M.; Poli, R.; Legzdins, P. *Chem.−Eur. J.* **1999**, *5*, 1598−1608.

**Figure 5.** ^{1}H NMR spectrum (300 MHz, 25 °C, pyridine-$d_5$) of the solution formed by thermolysis of Cp*Mo(NO)(CH$_2$CMe$_3$)(C$_6$H$_5$) (**6**) in pyridine-$d_5$. Resonances due to the complexes Cp*Mo(NO)(=CHCMe$_3$)(NC$_5$D$_5$) (**8**-$d_5$) and Cp*Mo(NO)($\eta^2$-C$_6$H$_4$)(NC$_5$D$_5$) (**9**-$d_5$) are indicated. Residual solvent protons are labeled with an asterisk, and $d_5$ labels are omitted for clarity.

alkylidene NMR resonances at $\delta$ 12.43 and 298.4 for the α-proton and the α-carbon of the neopentylidene ligand, respectively.[28] Interestingly, Cp*Mo(NO)(CH$_2$CMe$_3$)(CH$_2$-SiMe$_3$) (**2**) reacts in neat pyridine-$d_5$ solution in a similar manner to form primarily **8**-$d_5$ with concomitant elimination of tetramethylsilane. A small amount of neopentane is also evolved during this conversion, but no organometallic coproducts have yet been definitively identified.

The room-temperature thermolysis of **6** in neat PMe$_3$ for 24 h results in the formation of a brown solution containing Cp*Mo(NO)(=CHCMe$_3$)(PMe$_3$) that can be identified by its characteristic ^{1}H NMR spectrum. Interestingly, a similar thermolysis of **6** in pyridine affords an orange mixture of the alkylidene complex **8** and the benzyne complex Cp*Mo(NO)-($\eta^2$-C$_6$H$_4$)(NC$_5$H$_5$) (**9**) (eq 7). Monitoring of this reaction by



(7)
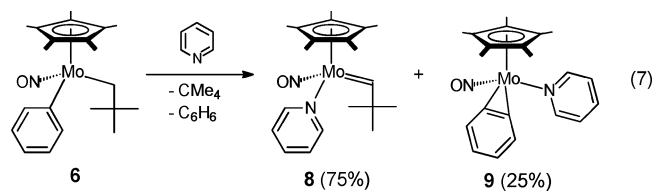
^{1}H NMR spectroscopy in pyridine-$d_5$ reveals that **8**-$d_5$ is formed preferentially (in an approximate 3:1 ratio), and signals due to liberated neopentane and benzene are also detectable in the ^{1}H NMR spectrum of the crude reaction mixture (Figure 5). The aromatic region of the ^{1}H NMR spectrum of **9**-$d_5$ exhibits inequivalent benzyne signals with overlapping multiplets at $\delta$ 7.48 (2H), 7.78 (1H), and 7.89 (1H). The ^{13}C{^{1}H} NMR spectrum shows two low-field signals at $\delta$ 158.4 and 162.2 which correspond to the ipso carbon atoms of the benzyne ligand as well as four other benzyne carbon signals. The line shapes of these signals are invariant from 20 to 85 °C, thereby indicating that **9** is stereochemically rigid in pyridine-$d_5$ and that the Mo-$\eta^2$-C$_6$H$_4$ linkage is static. Also, pyridine ligand exchange apparently does not occur, since the NMR spectra of **9** in pyridine-$d_5$ at 85 °C are invariant with time.
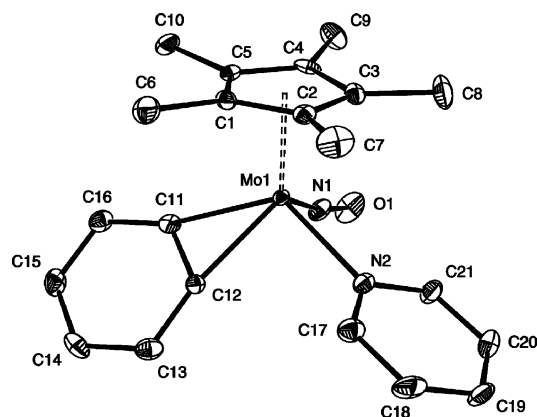


**Figure 6.** ORTEP plot of the solid-state molecular structure of Cp*Mo-(NO)($\eta^2$-C$_6$H$_4$)(NC$_5$H$_5$) (**9**) with 50% probability ellipsoids. Selected bond lengths (Å) and angles (deg): Mo(1)−C(11) = 2.124(4), Mo(1)−C(12) = 2.153(4), C(11)−C(12) = 1.356(6), Mo(1)−N(1) = 1.774(4), N(1)−O(1) = 1.228(5), Mo(1)−N(1)−O(1) = 169.2(4), and C(11)−Mo(1)−C(12) = 36.96(16).

The benzyne complex **9** can be readily isolated from the final reaction mixture by fractional crystallization from ether, and it is obtained as a canary yellow powder in 17% yield based on **6** (i.e., a theoretical maximum yield of 25%). Recrystallization of **9** from benzene provides yellow needles suitable for analysis by single-crystal X-ray diffraction, and the resulting ORTEP diagram of the solid-state molecular structure of **9** is shown in Figure 6. As anticipated, the dihedral angle between the planar benzyne ligand and the Mo(1)−C(11)−C(12) plane is only 1.2-(2)°. The length of the benzyne C−C bond coordinated to the molybdenum center is 1.356(6) Å, while the other C−C bond distances in this ligand range from 1.374(6) to 1.394(6) Å with an average value of 1.383 Å. The two Mo−C(benzyne) distances of 2.124(4) and 2.153(4) Å are unequal and larger than those (2.011 and 2.056 Å) extant in the only previously reported molybdenum aryne complex, namely Mo($\eta^2$-2-MeC$_6$H$_3$)(2-MeC$_6$H$_4$)$_2$(PMe$_2$Ph)$_2$.[29] The infrared spectrum of **9** in KBr

(28) Nugent, W. A.; Mayer, J. M. *Metal−Ligand Multiple Bonds*; Wiley: New York, 1988; Chapter 4.

(29) Koschmieder, S. U.; McGilligan, B. S.; McDermott, G.; Arnold, J.; Wilkinson, G.; Hussain-Bates, B.; Hursthouse, M. B. *J. Chem. Soc., Dalton Trans.* **1990**, 3427−3433.
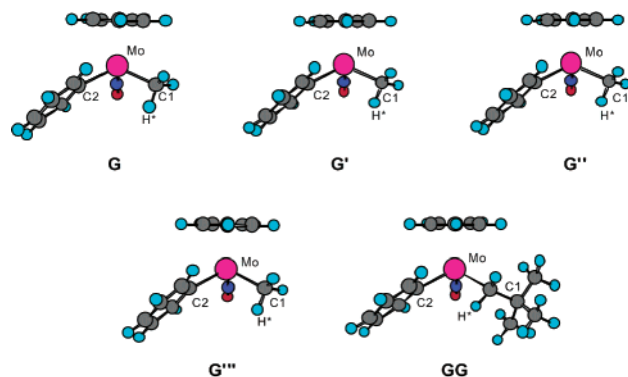
**Scheme 2**
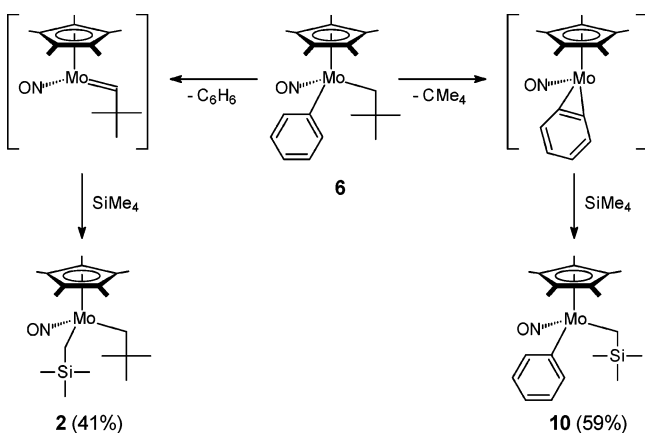


exhibits strong absorptions at 1537 and 1583 cm$^{-1}$, which can be assigned to $\nu_{NO}$ and $\nu_{C\equiv C}$ stretching frequencies, respectively.

**C–H Bond-Activation Chemistry Initiated by 6.** Solutions of **6** in C$_6$D$_6$ are converted to primarily **6**-$d_6$ (27%) and **7**-$d_6$ (68%), along with traces of Cp*Mo(NO)(C$_6$D$_5$)$_2$ (**7**-$d_{10}$) (eq 8). Thermolysis of **6** in tetramethylsilane at room temperature for 48 h results in the clean formation of **2** (41%) and Cp*Mo-(NO)(CH$_2$SiMe$_3$)(C$_6$H$_5$) (**10**, 59%) as measured after 70% conversion (Scheme 2).
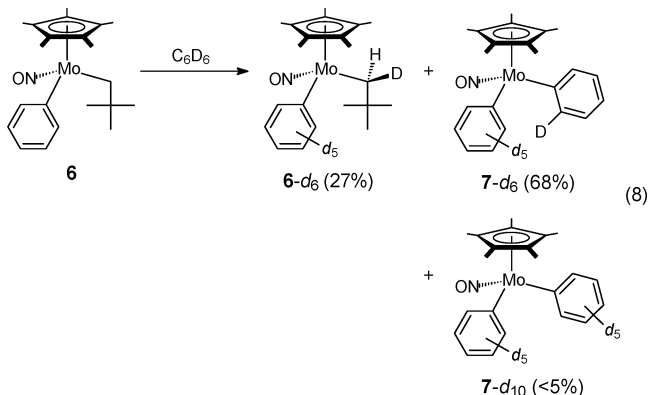


The distribution of products resulting from the reactions of hydrocarbons with **6** thus appears to be dependent on the nature of the hydrocarbon substrate, possibly due to the presence of σ- or π-hydrocarbon complexes on the reaction coordinates of the alkylidene and benzyne intermediates. [This possibility is specifically addressed during the theoretical investigations summarized in the next section.] Although the insertion of unsaturated small molecules into a metal–carbon bond of a benzyne complex is a well-established phenomenon, only a relatively few benzyne complexes (either isolated or invoked) have been reported to undergo intermolecular C–H bond activation processes and then usually at temperatures in excess of 100 °C.[16,30–32] In addition, Jones has implicated various benzyne species during the C–F bond activation of fluorinated arenes,[20,33] and Hughes recently prepared the first tetrafluorobenzyne complexes via *ortho*-fluoride abstraction from pentafluorophenyl ligands.[34]

(30) Erker, G. *J. Organomet. Chem.* **1977**, *134*, 189–202.
(31) Fagan, P. J.; Manriquez, J. M.; Maatta, E. A.; Seyam, A. M.; Marks, T. J. *J. Am. Chem. Soc.* **1981**, *103*, 6650–6667.
(32) (a) Hartwig, J. F.; Andersen, R. A.; Bergman, R. G. *J. Am. Chem. Soc.* **1989**, *111*, 2717–2719. (b) Hartwig, J. F.; Bergman, R. G.; Andersen, R. A. *J. Am. Chem. Soc.* **1991**, *113*, 3404–3418.



**Figure 7.** DFT optimized geometries of CpMo(NO)(C$_6$H$_5$)(CH$_3$) (**G**–**G'''**) and CpMo(NO)(C$_6$H$_5$)(CH$_2$CMe$_3$) (**GG**).

**Table 2.** DFT Optimized Structural Parameters for CpMo(NO)(C$_6$H$_5$)(CH$_3$) (**G**–**G'''**) and CpMo(NO)(C$_6$H$_5$)(CH$_2$CMe$_3$) (**GG**) (see Figure 7)

| parameter | G | G' | G'' | G''' | GG |
|---|---|---|---|---|---|
| Mo–C1 | 2.143 | 2.147 | 2.142 | 2.160 | 2.131 |
| Mo–C2 | 2.117 | 2.121 | 2.124 | 2.133 | 2.130 |
| Mo–H* | 2.594 | 2.597 | 2.553 | 2.593 | 2.379 |
| C1–H* | 1.106 | 1.106 | 1.107 | 1.102 | 1.121 |
| Mo–N | 1.773 | 1.768 | 1.763 | 1.780 | 1.772 |
| N–O | 1.240 | 1.243 | 1.204 | 1.193 | 1.242 |
| C1–Mo–C2 | 113.8 | 112.5 | 114.4 | 114.9 | 111.3 |
| Mo–C1–H* | 101.1 | 101.1 | 98.5 | 100.2 | 88.4 |
| Mo–N–O | 173.8 | 173.7 | 172.4 | 172.7 | 172.2 |

**Theoretical Investigations into C–H Activations by CpMo(NO) Complexes. A. Optimal Structures of CpMo(NO)-(C$_6$H$_5$)(alkyl) Complexes.** The molecular structure of CpMo-(NO)(C$_6$H$_5$)(CH$_3$) optimized by DFT calculations with LanL2DZ (**G**), SDD (**G'**), LanL2DZ-II (**G''**), or LanL2DZ-III (**G'''**) basis sets and that of CpMo(NO)(C$_6$H$_5$)(CH$_2$CMe$_3$) optimized by using the LanL2DZ basis set (**GG**) are shown in Figure 7. Intramolecular geometrical parameters of these structures are summarized in Table 2. The Cp–Mo, Mo–NO, and Mo–C$_6$H$_5$ intramolecular dimensions of structure **G** are generally comparable to those extant in the solid-state molecular structure of Cp*Mo(NO)(CH$_2$CMe$_3$)(C$_6$H$_5$) (**6**) shown in Figure 3. One of the methyl C–H bonds in **G**, namely C1–H*, is distorted toward the Mo atom in an orientation consistent with there being an interaction between this C–H bond and the vacant metal-based d orbitals.[35] Thus, the Mo–C1–H* angle (101.1°) is smaller than the normal value (109.5°) expected for an sp$^3$-hybridized C atom, and the Mo–H* distance (2.594 Å) is distinctly shorter than the others. Nevertheless, the extent of this calculated α-agostic interaction is significantly lower than that evident in the X-ray structure of **6**, in which the Mo–C1–H* angle and the Mo–H* distance are 78(2)° and 2.13(3) Å, respectively. The use of larger basis sets such as LanL2DZ-II or LanL2DZ-III instead of the normal LanL2DZ basis set only alters the extent of the α-agostic interaction slightly. Thus, the Mo–C1–H* angles extant in structures **G''** (98.5°) and **G'''** (100.2°) are slightly more acute than that in **G**, while, in the **G'**

(33) (a) Edelbach, B. L.; Kraft, B. M.; Jones, W. D. *J. Am. Chem. Soc* **1999**, *121*, 10327–10331. (b) Kraft, B. M.; Lachicotte, R. J.; Jones, W. D. *Organometallics* **2002**, *21*, 727–731.
(34) (a) Hughes, R. P.; Williamson, A.; Sommer, R. D.; Rheingold, A. L. *J. Am. Chem. Soc.* **2001**, *123*, 7443–7444. (b) Hughes, R. P.; Laritchev, R. B.; Williamson, A.; Incarvito, C. D.; Zakharov, L. N.; Rheingold, A. L. *Organometallics* **2002**, *21*, 4873–4885.
(35) Poli, R.; Smith, K. M. *Organometallics* **2000**, *19*, 2858–2867.
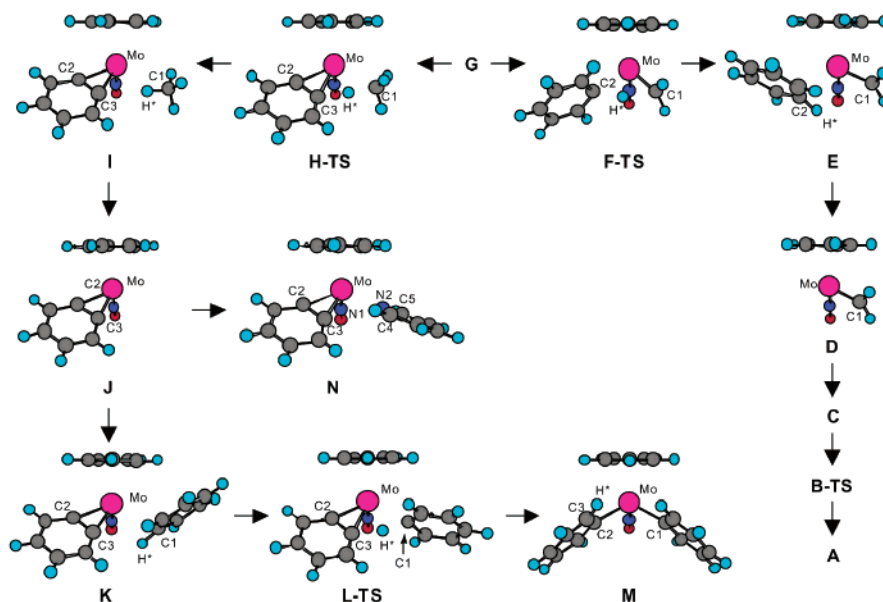
**Figure 8.** DFT optimized geometries of complexes in the CpMo(NO)(C$_6$H$_5$)(CH$_3$) (**G**) system.

structure optimized by the use of the SDD basis set, it is very close to that in **G** (Table 2).

On the other hand, the structure of the phenyl neopentyl complex **GG** optimized by the B3LYP/LanL2DZ calculations involves one strongly agostic methylene hydrogen. Indeed, the computed acute Mo–C1–H* angle (88.4°) and the short Mo–H* distance (2.379 Å) indicate that **GG** is a better model for the actual complex **6**, probably for both steric and electronic reasons. For instance, the inductive effect of a $^t$Bu group would increase the basicity of the methylene C–H linkages and enhance the interaction between the α-hydrogen and the strongly Lewis-acidic[9] molybdenum center. The present study clearly shows that the use of the simplified model **G** results in an underestimation of α-agostic interactions which often play very important roles during the cleavage of α-C–H bonds by metal-assisted abstraction pathways.[8]

Based on these initial findings, we next examined the intermolecular C–H bond activation pathways initiated by the neopentyl phenyl complex **6** by the use of both models, **G** and **GG**, to assess what effects the simplification of the alkyl ligands has on these pathways. The LanL2DZ basis set was used during the following calculations in order to minimize computational expense. At this point, it may also be noted that, in general, the HOMOs and LUMOs of the various structures optimized during this work resemble those described by Poli and Smith during their theoretical investigations of related systems.[35]

**B. C–H Activations Initiated by CpMo(NO)(C$_6$H$_5$)(CH$_3$).** Optimal geometries have been determined for various species included in the activation processes, and the results of these computations are presented in Figure 8 and Table S1 of the Supporting Information. A π-benzene adduct of the carbene fragment CpMo(NO)(=CH$_2$) has been successfully located as a distinct intermediate (**E**) for the process involving eventual benzene expulsion.[36] Another stable intermediate (**E′**) with the π-benzene ligand positioned away from the Cp ring has also been found, and its calculated energy is almost the same as that of **E**. Similar stable intermediates have been found during the

theoretical studies of CpW(NO)R$_2$ systems.[36] The transition state from the methyl phenyl complex **G** to **E** via a one-step, σ-bond metathesis pathway is a late one (**F-TS**), with the hydrogen atom being transferred being more than halfway to the H-acceptor carbon.

On the other hand, for the pathway involving methane loss from the methyl phenyl reactant, a stable σ-methane benzyne intermediate **I** has been found. The methane ligand is coordinated in an η$^2$ fashion to the metal center with Mo–H and Mo–C bond distances of 2.211 Å and 2.877 Å, respectively. Both distances are slightly longer than those previously computed for the corresponding methane methylene intermediate, CpMo-(NO)(σ-CH$_4$)(=CH$_2$) (**C**).[35] The transition state **H-TS** from **G** to **I** is a very late one in which the formation of the benzyne and methane ligands is almost complete. Thus, the distance between the transferring hydrogen, H*, and the methyl acceptor is only 1.389 Å, whereas that between H* and C3 is 1.554 Å. In a related theoretical study of plausible mechanisms for generating tungsten carbene species from Cp′W(NO)(CH$_3$)$_2$ (Cp′ = Cp or Cp*), Fan and Hall[37] found the stable intermediates Cp′W(NO)(H)(=CH$_2$)(CH$_3$) that result from α-H oxidative addition. Nevertheless, they concluded that the one-step, σ-bond metathesis-like mechanism is the preferred one. We therefore attempted to locate CpMo(NO)(H)(η$^2$-C$_6$H$_4$)(CH$_3$), a stable intermediate resulting from the oxidative addition of a β-hydrogen of the phenyl ring, during the course of the transformation from **G** to **I**. However, such a species was not found at the present calculation level even after extensive searching with various initial reactant geometries. Finally, the transition state **L-TS** has been located during the course of the reaction from the π-benzene benzyne intermediate **K** to the diphenyl complex **M**. The molecular structure of **L-TS** is very similar to that of the benzene intermediate **K**. Remarkably, the structure of the pyridine adduct of the benzyne intermediate, **N**, optimized by the B3LYP/LanL2DZ calculation is almost the same as the X-ray structure of **9**. Thus, the computed C2–C3 bond length of the benzyne ligand is 1.364 Å, only slightly longer than the actual value (1.356(6) Å). The other C–C bond distances in

(36) Adams, C. S.; Legzdins, P.; McNeil, W. S. *Organometallics* **2001**, *20*, 4939–4955.

(37) Fan, Y.; Hall, M. B. *J. Chem. Soc., Dalton Trans.* **2002**, 713–718.

**Table 3.** Relative Energies of Complexes in the CpMo(NO)(C₆H₅)(CH₃) Model System (see Figure 9)

| complex | ΔE (kcal mol⁻¹) | ΔG (kcal mol⁻¹) |
|---|---|---|
| **D** | 29.53 | 18.86 |
| **E** | 16.73 | 16.18 |
| **E′** | 16.44 | 16.82 |
| **F-TS** | 29.45 | 31.02 |
| **G** | 0.00 | 0.00 |
| **H-TS** | 33.62 | 34.96 |
| **I** | 25.11 | 23.84 |
| **J** | 27.85 | 17.50 |
| **K** | 19.02 | 19.04 |
| **L-TS** | 26.52 | 28.90 |
| **M** | −4.18 | −3.69 |
| **N** | −6.83 | −5.54 |
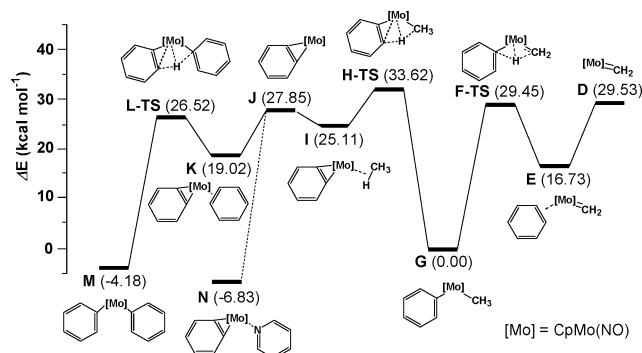


**Figure 9.** Reaction profile showing the calculated energies of complexes derived from CpMo(NO)(C₆H₅)(CH₃) (**G**) (see Table 3).

the benzyne ligand (1.399−1.420 Å), the two Mo−C(benzyne) distances (2.115 and 2.150 Å), and the coordination geometry of the pyridine ligand (e.g., Mo−N2 = 2.227 Å) also compare very well with those found in the X-ray structure (Figure 6).

The data summarized in Table 3 and presented pictorially in Figure 9 show the complete energy profile accompanying these C−H activation processes originating at **G**. The calculated activation barrier for the generation of the active benzyne intermediate from **G** (33.62 kcal mol⁻¹) is slightly higher than that for the methylene intermediate (29.45 kcal mol⁻¹), and it is consistent with the results obtained in competition experiments (vide supra). The benzyne intermediate stabilized by π-coordinated benzene (**K**) is 19.02 kcal mol⁻¹ less stable than the reactant **G**, and the energy of the transition state **L-TS** is only 7.50 kcal mol⁻¹ higher than that of **K**. This result indicates that once the reactive benzyne intermediate is formed in benzene solution, the reaction spontaneously proceeds to form the thermodynamically stable diphenyl complex **M**. Conversely, the diphenyl complex needs to overcome a relatively large barrier (30.70 kcal mol⁻¹) in order to generate an active benzyne intermediate. Finally, the low energy level of the pyridine adduct **N** (−6.83 kcal mol⁻¹) indicates the high thermal stability of such Lewis-base adducts, a feature discussed previously by other investigators.[35]

**C. C−H Activations Initiated by CpMo(NO)(C₆H₅)(CH₂CMe₃).** All the optimized structures are shown in Figure 10, and their key structural parameters are summarized in Table 4 and Table S2 in the Supporting Information. The relative energies of the various species are collected in Table 5 and are presented pictorially in Figure 11. The Mo−C1 bond lengths in the optimal structures of **DD**, **EE**, and **FF-TS** are slightly

longer (∼0.01 Å) than those found in the phenyl methyl system. In **FF-TS** the Mo−H distance is much shorter (by more than 0.02 Å) than that in **F-TS**. Remarkably, the employment of a model including a neopentyl group greatly reduces the calculated barrier for the formation of a reactive alkylidene intermediate. Thus, the relative energy of the transition state **FF-TS** is 5.58 kcal mol⁻¹ lower than that calculated for the simpler methyl system (**F-TS**). On the other hand, the presence of a bulky neopentyl ligand does not result in any significant changes of the activation barrier for the formation of the benzyne intermediate. Hence, the relative energy of the transition state **HH-TS** is 34.70 kcal mol⁻¹, only slightly higher than that of **H-TS** (33.62 kcal mol⁻¹). As a result, the barrier for the generation of the active benzyne intermediate is 10.83 kcal mol⁻¹ higher than that for the neopentylidene species, again indicating that in the neopentyl phenyl complex α-hydrogen abstraction to form the Mo=CHCMe₃ linkage is more facile than the β-hydrogen elimination to form the benzyne species. It may also be noted that the optimized structure of the pyridine adduct of the alkylidene intermediate **OO** (a known compound)[6b] compares well with the solid-state molecular structure of the corresponding complex **8** (Figure 4). Thus, the Mo−C1 bond length (1.951 Å), the Mo−C1−C(tBu) angle (138.4°), and the coordination geometry of the pyridine ligand (i.e., Mo−N2 = 2.205 Å) compare very well with those found in the experimentally determined structure. Finally, as for **N**, the computed energy level of **OO** is relatively low (−13.52 kcal mol⁻¹), again indicating its relatively high thermal stability.

**D. C−H Activations Initiated by CpMo(NO)(CH₂CMe₃)₂.** In addition to investigating the parallel generation of the active intermediates from the alkyl phenyl complexes, we have also studied mechanisms for generating molybdenum alkylidene species from CpMo(NO)(CH₂CMe₃)₂ (**AA**) by neopentane elimination. Apart from the methyl groups on the Cp ring, the structural parameters of **AA** closely resemble those in the solid-state molecular structure of **1** (Figure 1) except for the geometries of the α-hydrogens. The optimized structure of CpMo(NO)(CH₂CMe₃)₂ involves two "moderately agostic" α-hydrogens (Mo to α-H = 2.484 Å and 2.478 Å). Nevertheless, the extent of α-agostic interaction in **AA** is significantly larger than those found in previous studies employing model dimethyl complexes.[35,37] As summarized in Table 5, the activation energy for the one-step transformation of **AA** into the stable σ-neopentane neopentylidene intermediate **CC** is calculated to be 27.34 kcal mol⁻¹ (27.58 kcal mol⁻¹ based on ΔEₒ calculated from the sum of electronic and zero-point energies) According to the previous report,[35] the computed activation barrier from CpMo(NO)(CH₃)₂ (**A**) to CpMo(NO)(=CH₂)(σ-CH₄) (**C**) is 32.62 kcal mol⁻¹ based on ΔEₒ. A comparison of these data clearly indicates that the use of "unsimplified" models greatly lowers the barrier for the α-hydrogen elimination pathway. Hence, it is worth noting at this point that while the insights provided by computations can be very useful, the results obtained using simplified models such as Cp′M(NO)(CH₃)₂ in place of the actual and more complicated bis(alkyl) compounds should be interpreted with caution. In fact, in this particular system the dimethyl complexes do not even exhibit α-H elimination chemistry, spontaneously converting instead to their
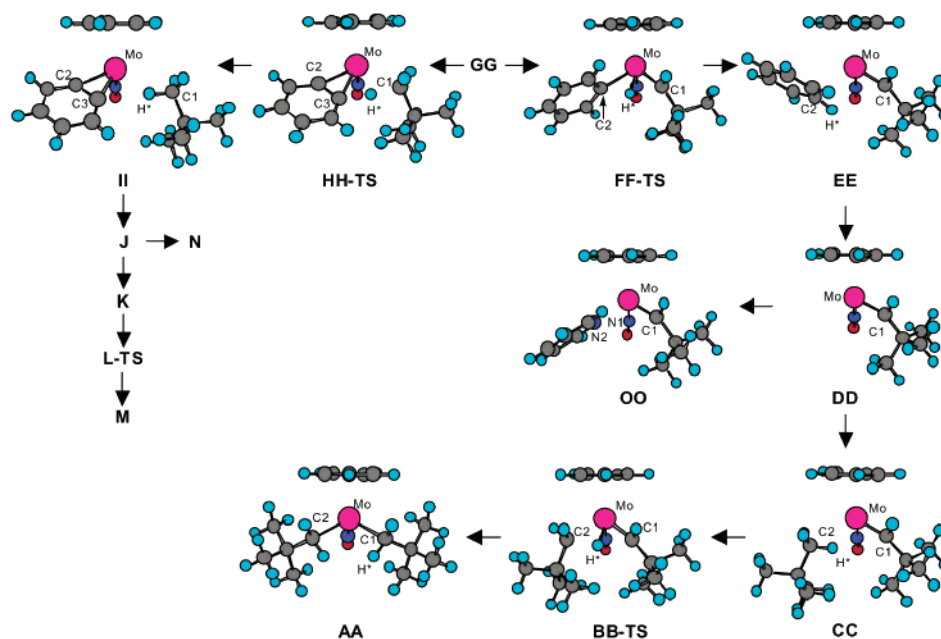
**Figure 10.** DFT optimized geometries of complexes in the CpMo(NO)($C_6H_5$)($CH_2CMe_3$) (**GG**) system.

**Table 4.** DFT Optimized Structural Parameters for Neopentane σ-Complexes **HH-TS** and **II** (see Figure 10)

| parameter | HH-TS | II |
|---|---|---|
| Mo—C1 | 2.407 | 2.905 |
| Mo—C2 | 2.100 | 2.107 |
| Mo—C3 | 2.228 | 2.138 |
| Mo—H* | 1.861 | 2.156 |
| C1—H* | 1.460 | 1.123 |
| C3—H* | 1.534 | 2.492 |
| Mo—N1 | 1.784 | 1.786 |
| N—O | 1.237 | 1.238 |
| C1—Mo—C2 | 116.9 | 127.3 |
| C1—Mo—C3 | 80.1 | 90.1 |
| Mo—N—O | 172.6 | 173.2 |

**Table 5.** Relative Energies of Complexes in the CpMo(NO)($C_6H_5$)($CH_2CMe_3$) Model System (see Figure 11)

| complex | $\Delta E$ (kcal mol$^{-1}$) | $\Delta G$ (kcal mol$^{-1}$) |
|---|---|---|
| **AA** | 4.58 | 4.48 |
| **BB-TS** | 31.92 | 33.41 |
| **CC** | 14.79 | 13.39 |
| **DD** | 24.60 | 12.51 |
| **EE** | 12.38 | 11.00 |
| **FF-TS** | 23.87 | 24.44 |
| **GG** | 0.00 | 0.00 |
| **HH-TS** | 34.70 | 36.30 |
| **II** | 22.09 | 19.74 |
| **J** | 29.42 | 17.39 |
| **K** | 20.59 | 18.92 |
| **L-TS** | 28.09 | 28.78 |
| **M** | −2.61 | −3.81 |
| **OO** | −13.52 | −14.18 |

oxo imido isomers, Cp′M[N(CH$_3$)](O)(CH$_3$), via nitrosyl N—O bond cleavage under the experimental conditions employed.[38]

In summary, thermolysis of the neopentyl phenyl complex **6** in hydrocarbon solutions affords products via both the neopentylidene and benzyne intermediates at ambient temperatures. However, the products are formed in different ratios depending

(38) Sharp, W. B.; Daff, P. J.; McNeil, W. S.; Legzdins, P. *J. Am. Chem. Soc.* **2001**, *123*, 6272−6282.

on the substrates involved, thereby indicating that the rate of traversal of the two competitive C—H bond-activation pathways depends on the nature of the hydrocarbon substrates. The theoretical part of this work clearly indicates the presence of σ- or π-hydrocarbon complexes on the reaction coordinates of the alkylidene and the benzyne intermediates.[13,36] Consistent with the calculations is the observation that trapping of the intermediates with Lewis bases such as pyridine results in more of the trapped neopentylidene complex, since it is more readily formed from **6**. However, the neopentylidene intermediate is computed to effect C—H bond activations more slowly, and thus, with substrates such as benzene and tetramethylsilane, the products resulting from the benzyne intermediate should predominate, as is indeed observed experimentally. In other words, the less abundant intermediate is responsible for the majority of the C—H activated products. This qualitative agreement of theory and experiment is gratifying, especially since the theoretical calculations were effected on the model Cp complexes in the gas phase rather than the actual Cp* complexes in solutions for which solvent effects would also be expected to play a role.

## Epilogue

Our initial investigations of the thermal reactivity of **1** and **6** have revealed several unique characteristics of C—H bond activation by the reactive molybdenum alkylidene and benzyne complexes, Cp*Mo(NO)(=CHCMe$_3$) and Cp*Mo(NO)($\eta^2$-C$_6H_4$). First, the activation of C—H bonds occurs at room temperature via the 1,2-C—H addition of the substrate to the Mo=C double bond of Cp*Mo(NO)(=CHCMe$_3$) with a slight kinetic preference for the strongest C—H bond. Second, parallel modes of C—H bond activation can be initiated from **6** by elimination of either alkane or arene, resulting in the simultaneous formation of the Cp*Mo(NO)(=CHCMe$_3$) and Cp*Mo-(NO)($\eta^2$-C$_6H_4$) intermediates, both of which can activate C—H bonds. It is thus not unreasonable to expect that thermally induced α-H elimination of various hydrocarbons from other mixed-hydrocarbyl congeners of the large family of available
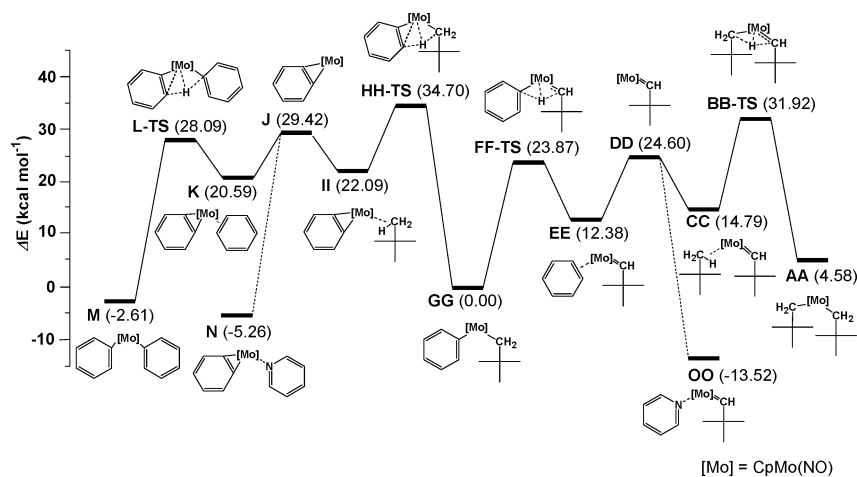
**Figure 11.** Reaction profile showing the calculated energies of complexes derived from CpMo(NO)(C$_6$H$_5$)(CH$_2$CMe$_3$) (**GG**) (see Table 5).

Cp*Mo(NO)(R)(R′) complexes will provide a wide variety of coordinatively unsaturated complexes suitable for the activation of hydrocarbons in unprecedented ways. Our studies in this regard with these and related complexes are currently in progress, and the results of these investigations will be reported in due course.

## Experimental Section

**General Methods.** All reactions and subsequent manipulations were performed under rigorously anaerobic and anhydrous conditions utilizing either high vacuum or an atmosphere of prepurified argon or dinitrogen with conventional gloveboxes and vacuum-line Schlenk techniques. The gloveboxes used were Innovative Technologies Lab-Master 100 and MS-130 BG dual-station models equipped with freezers maintained at −30 °C. Thermolysis reactions were performed in thick-walled glass bombs equipped with Kontes greaseless stopcocks, and NMR spectroscopic analyses were conducted in J. Young NMR tubes.

All solvents were dried and distilled prior to use or vacuum transferred directly from the appropriate drying agent. Hydrocarbons and diethyl ether were distilled from sodium benzophenone ketyl, tetrahydrofuran was distilled from molten potassium, and dichloromethane and chloroform were distilled from calcium hydride. Deuterated solvents were purchased from Cambridge Isotope Laboratories and then degassed and vacuum-transferred from K (C$_6$D$_6$), Na (toluene-$d_8$), or activated 4 Å molecular sieves (CD$_2$Cl$_2$). Trimethylphosphine (Aldrich) was dried and stored over potassium. Pyridine was dried over KOH and distilled onto activated 4 Å molecular sieves. Celite and neutral alumina I (60−325 mesh) were oven-dried and cooled under vacuum prior to use.

Infrared spectra were recorded on an ATI Mattson Genesis Series FT-IR spectrometer. NMR spectra were recorded at room temperature, unless otherwise noted, on Bruker AV300 or AMX 500 spectrometers. $^1$H and $^{13}$C chemical shifts are recorded in ppm relative to the residual proton or natural-abundance carbon signal(s) of the solvents employed; coupling constants are reported in Hz. $^2$H{$^1$H} NMR signals were referenced to C$_6$H$_5$D ($\delta$ 7.15). Correlation and assignment of $^1$H and $^{13}$C NMR resonances were aided by 2D HMQC and HMBC experiments when necessary. Low-resolution mass spectra (EI, 70 eV) were recorded by the staff of the UBC mass spectrometry facility using a Kratos MS-50 spectrometer. Elemental analyses were performed by Canadian Microanalytical Service Ltd., Delta, B.C., Canada.

**Preparation of Cp*Mo(NO)(CH$_2$CMe$_3$)$_2$ (1).** This complex was prepared by a modification of the previously reported method.[10,39] To a Schlenk tube containing [Cp*Mo(NO)Cl$_2$]$_2$ (1.156 g, 1.74 mmol) and

(39) Legzdins, P.; Young, M. A.; Batchelor, R. J.; Einstein, F. W. B. *J. Am. Chem. Soc.* **1995**, *117*, 8798−8806.

(Me$_3$CCH$_2$)$_2$Mg·$x$(dioxane) (0.486 g, 1.85 mmol) at −196 °C was added THF (40 mL) by vacuum transfer. The resulting brown suspension was warmed to 0 °C and stirred for 20 min, whereupon a purple solution formed. The volatiles were then removed from the reaction mixture under reduced pressure. The flask containing the residue was charged with a second portion of (Me$_3$CCH$_2$)$_2$Mg·$x$(dioxane) (0.462 g, 1.76 mmol), and Et$_2$O (40 mL) was added by vacuum transfer at −196 °C. The resulting mixture was allowed to warm to room temperature, and the red suspension was stirred for 30 min. The solvent was removed from the final reaction mixture in vacuo, and the residue was extracted with 4:1 hexanes/Et$_2$O (3 × 10 mL). The red extracts were filtered through a column of neutral alumina (3 × 1 cm) supported on a medium-porosity frit, and the column was washed with 4:1 hexanes/Et$_2$O until the filtrate was colorless. The combined filtrates were concentrated and stored at −30 °C for 2 days to obtain burgundy needles of **1** (0.797 g, 56% in three crops).

Anal. Calcd for C$_{20}$H$_{37}$NOMo: C, 59.54; H, 9.24, N, 3.47. Found: C, 59.33; H, 9.51; N, 3.43. IR (Nujol): $\nu$(NO) 1599 (s) cm$^{-1}$. $^1$H NMR (toluene-$d_8$, 300 MHz, 0 °C) $\delta$ −1.06 (d, $^2J_{HH}$ = 11.7 Hz, 2H, C$H_{syn}$-HCMe$_3$), 1.37 (s, 18H, CMe$_3$), 1.50 (s, 15H, C$_5$Me$_5$), 2.96 (d, $^2J_{HH}$ = 11.7 Hz, 2H, C$H_{anti}$HCMe$_3$). Gated $^{13}$C NMR (toluene-$d_8$, 75.5 MHz, 0 °C): $\delta$ 9.5 (q, $^1J_{CH}$ = 127.2 Hz, C$_5$$Me_5$), 33.5 (q, $^1J_{CH}$ = 124.2 Hz, C$Me_3$), 38.7 (s, $C$Me$_3$), 97.4 (dd, $^1J_{CH}$ = 101 Hz, $^1J_{CH}$ = 125 Hz, CH$_2$), 109.3 (s, $C_5$Me$_5$). MS (EI, 100 °C): $m/z$ 405 [P$^+$].

**Preparation of Cp*Mo(NO)(CH$_2$CMe$_3$)(CH$_2$SiMe$_3$) (2).** A red solution of **1** (0.096 g, 0.24 mmol) in Me$_4$Si (8 mL) was stirred at room temperature for 30 h. The solution was then evaporated to dryness in vacuo, and the red solid was extracted with hexanes (5 mL). The extract was filtered through a column of neutral alumina, and the filtrate was stored at −30 °C for several days to induce the deposition of **2** as a red crystalline mass (0.032 g, 32%). The IR, NMR, and mass spectral data of these crystals were identical to those reported previously for **2**.[10]

**Preparation of Cp*Mo(NO)(CH$_2$CMe$_3$)($\eta^2$-CH$_2$C$_6$H$_3$-3,5-Me$_2$) (3).** A red solution of **1** (0.100 g, 0.249 mmol) in mesitylene (10 mL) was stirred at room temperature for 30 h. The final solution was taken to dryness in vacuo, and the solid orange residue was extracted with 10:1 hexanes/Et$_2$O (3 × 10 mL). The combined extracts were filtered through a column of neutral alumina (0.5 × 5 cm), and the filtrate was stored at −30 °C overnight to induce the deposition of **3** as yellow needles (0.030 g, 27%).

Anal. Calcd for C$_{24}$H$_{37}$MoN$_2$O: C, 63.84; H, 8.26; N, 3.10. Found: C, 63.85; H, 8.23; N, 3.05. IR (Nujol): $\nu$(NO) 1601 (s) cm$^{-1}$. $^1$H NMR (C$_6$D$_6$, 300 MHz, 25 °C) $\delta$ −2.48 (d, $^2J_{HH}$ = 12.4 Hz, 1H, C$H_{syn}$-HCMe$_3$), 1.12 (d, $^2J_{HH}$ = 12.4 Hz, 1H, C$H_{anti}$HCMe$_3$), 1.16 (s, CMe$_3$, 9H), 1.61 (s, C$_5$Me$_5$, 15H), 1.96 (s, C$_6$H$_3$$Me_2$, 6H), 2.01 (d, $^2J_{HH}$ = 4.7 Hz, 1H, C$H_{syn}$HC$_6$H$_3$Me$_2$), 3.43 (d, $^2J_{HH}$ = 4.7 Hz, 1H, C$H_{anti}$HC$_6$H$_3$-

Me$_2$), 5.94 (s, benzyl $H_{ortho}$, 2H), 7.06 (s, benzyl $H_{para}$, 1H). $^{13}$C{$^1$H} NMR (C$_6$D$_6$, 75 MHz, 25 °C) $\delta$ 10.6 (C$_5$Me$_5$), 21.1 (C$_6$H$_3$Me$_2$), 34.8 (CMe$_3$), 37.1 (CMe$_3$), 46.0 (CH$_2$C$_6$H$_3$Me$_2$), 57.8 (CH$_2$CMe$_3$), 108.4 (C$_5$-Me$_5$), 118.4 (benzyl $C_{ipso}$), 131.1 (benzyl $C_{ortho}$), 132.2 (benzyl $C_{para}$), 138.5 (benzyl $C_{meta}$). MS (EI, 100 °C): $m/z$ 453 [P$^+$].

**Thermal Reaction of 1 in *p*-Xylene.** A red solution of **1** (0.101 g, 0.251 mmol) in *p*-xylene (10 mL) was stirred at room temperature for 44 h. The final red solution was then taken to dryness in vacuo, and the solid residue was dissolved in C$_6$D$_6$ for analysis by $^1$H NMR spectroscopy. This analysis indicated the presence of Cp*Mo(NO)-(CH$_2$CMe$_3$)(C$_6$H$_3$-2,5-Me$_2$) (**4**, 73%) and Cp*Mo(NO)(CH$_2$CMe$_3$)($\eta^2$-CH$_2$C$_6$H$_4$-4-Me) (**5**, 27%). Attempts to separate complexes **4** and **5** by column chromatography were unsuccessful, but the mixture was sufficiently pure to afford an acceptable elemental analysis. Anal. Calcd for C$_{23}$H$_{35}$MoNO: C, 63.15; H, 8.06; N, 3.20. Found: C, 63.13; H, 7.62; N, 3.59. MS (EI, 120 °C): $m/z$ 439 [P$^+$].

Characterization data for **4**: $^1$H NMR (C$_6$D$_6$, 300 MHz, 25 °C) $\delta$ 1.24 (s, 9H, CMe$_3$), 1.39 (s, 3H, aryl CH$_3$), 1.53 (s, 15H, C$_5$Me$_5$), 1.55 (d, 1H, CH$_{syn}$H), 2.14 (d, 1H, CH$_{anti}$H), 2.16 (s, 3H, aryl CH$_3$), 6.87 (br d, $^3J_{HH}$ = 7.9 Hz, 1H, phenyl $H$), 7.09 (br d, $^3J_{HH}$ = 7.9 Hz, 2H, phenyl $H$). The methylene hydrogen doublets occurring at $\delta$ 1.55 (syn) and 2.14 (anti) are partially obscured by the aryl CH$_3$ and Cp* resonances, respectively, and $^2J_{HH}$ could not be determined.

Characterization data for **5**: $^1$H NMR (C$_6$D$_6$, 300 MHz, 25 °C) $\delta$ −2.83 (d, $^2J_{HH}$ = 12.4 Hz, 1H, CH$_{syn}$HCMe$_3$), 0.97 (d, $^2J_{HH}$ = 12.4 Hz, 1H, CH$_{anti}$HCMe$_3$), 1.19 (s, 9H, CMe$_3$), 1.57 (s, 15H, C$_5$Me$_5$), 2.00 (d, $^2J_{HH}$ = 4.9 Hz, 1H, CH$_{syn}$HAr), 2.13 (s, 3H, aryl CH$_3$), 3.36 (d, $^2J_{HH}$ = 4.9 Hz, 1H, CH$_{anti}$HAr), 6.19 (d, $^3J_{HH}$ = 7.9 Hz, 2H, phenyl $H$), 6.59 (d, $^3J_{HH}$ = 7.9 Hz, 2H, phenyl $H$). These data are consistent with those previously reported for this complex in CDCl$_3$.$^{12b}$

**Thermal Reaction of 1 in Benzene.** A red solution of **1** (0.205 g, 0.509 mmol) in C$_6$H$_6$ (10 mL) was stirred at room temperature for 30 h. The final red-purple solution was taken to dryness in vacuo, the violet residue was extracted with pentane (5 × 5 mL), and the combined extracts were filtered through a column of alumina (1 × 2 cm) supported on a medium-porosity glass frit. The filtrate was concentrated under reduced pressure to the point of incipient crystallization and was then stored at −30 °C. After 12 h, the solution had deposited wine red crystals of analytically pure Cp*Mo(NO)(CH$_2$CMe$_3$)(C$_6$H$_5$) (**6**) (0.056 g, 27%).

The solid remaining after pentane extraction was dissolved in Et$_2$O (5 mL), and the solution was filtered through a column of Celite (0.5 × 2 cm) supported on glass wool. The column was washed with Et$_2$O (3 × 5 mL), and the combined filtrates were concentrated under reduced pressure to the point of incipient crystallization. Violet needles (0.064 g, 30%) of Cp*Mo(NO)(C$_6$H$_5$)$_2$ (**7**) were deposited after the solution had been stored at −30 °C for several hours

Characterization data for **6**. Anal. Calcd for C$_{21}$H$_{31}$MoNO: C, 61.61; H, 7.63; N, 3.42. Found: C, 61.51; H, 7.91; N, 3.38. IR (KBr): $\nu$(NO) 1612 (s) cm$^{-1}$. $^1$H NMR (C$_6$D$_6$, 300 MHz, 25 °C) $\delta$ −1.75 (d, $^2J_{HH}$ = 9.7 Hz, 1H, CH$_{syn}$H), 1.25 (s, 9H, CMe$_3$), 1.51 (s, 15H, C$_5$Me$_5$), 4.77 (d, $^2J_{HH}$ = 9.7 Hz, 1H, CH$_{anti}$H), 7.07 (m, 1H, phenyl $H_{para}$), 7.16 (m, 2H, phenyl $H_{meta}$), 7.57 (d, $^3J_{HH}$ = 6.7 Hz, 2H, phenyl $H_{ortho}$). $^{13}$C{$^1$H} NMR (C$_6$D$_6$, 75 MHz, 25 °C) $\delta$ 10.0 (C$_5$Me$_5$), 33.2 (CMe$_3$), 41.3 (CMe$_3$), 111.1 (C$_5$Me$_5$), 114.5 (CH$_2$), 127.3 (phenyl $C_{para}$), 127.6 (phenyl $C_{meta}$), 135.4 (phenyl $C_{ortho}$), 180.1 (phenyl $C_{ipso}$). MS (EI, 120 °C): $m/z$ 411 [P$^+$], 381 [P$^+$ − NO].

The NMR and IR spectroscopic data for **7** matched those previously reported for the compound isolated from the reaction of [Cp*Mo(NO)-Cl($\mu$-Cl)]$_2$ with (C$_6$H$_5$)$_2$Mg·$x$(dioxane).$^{14}$ However, satisfactory elemental analyses for this compound are reported here for the first time. Anal. Calcd for C$_{22}$H$_{25}$MoNO: C, 63.61; H, 6.07; N, 3.37. Found: C, 63.40; H, 5.94; N, 3.34.

**Preparation of Cp*Mo(NO)(CHDCMe$_3$)(C$_6$D$_5$) (6-$d_6$).** A red solution of **1** (0.100 g, 0.248 mmol) in C$_6$D$_6$ (8 mL) was stirred at room temperature for 16 h. The final solution was taken to dryness in

vacuo, the dark red residue was extracted with hexanes (2 × 5 mL), and the extracts were filtered through a column of neutral alumina (0.5 × 5 cm) supported on glass wool. The filtrate was stored at −30 °C overnight to induce the deposition of red blocks of **6**-$d_6$ (0.064 g, 62%).

Anal. Calcd for C$_{21}$H$_{25}$D$_6$MoNO: C, 60.71; N, 3.37. Found: C, 60.56; N, 3.38. IR (KBr): $\nu$(NO) 1611 (s) cm$^{-1}$. $^1$H NMR (C$_6$D$_6$, 300 MHz, 25 °C) $\delta$ 1.24 (s, 9H, CMe$_3$), 1.51 (s, 15H, C$_5$Me$_5$), 4.66 (s, 1H, CDH$_{anti}$). $^2$H{$^1$H} NMR (C$_6$D$_6$, 77 MHz, 25 °C) $\delta$ −1.76 (br s, CD$_{syn}$H), 7.15 (s, C$_6$D$_6$), 7.10 (br m, overlapping D$_{meta}$ and D$_{para}$), 7.60 (br m, D$_{ortho}$). $^{13}$C{$^1$H} NMR (C$_6$D$_6$, 75 MHz, 25 °C) $\delta$ 10.0 (C$_5$Me$_5$), 33.4 (CMe$_3$), 41.1 (CMe$_3$), 111.1 (C$_5$Me$_5$), 112.6 (m, CHD), 126.5 (t, $^1J_{CD}$ = 14.6 Hz, phenyl $C_{para}$), 134.7 (t, $^1J_{CD}$ = 24.1 Hz, phenyl $C_{ortho}$), 180.1 (phenyl $C_{ipso}$). Additional phenyl signals ($C_{meta}$) are obscured by the benzene-$d_6$ peak. MS (EI, 150 °C): $m/z$ 417 [P$^+$].

The thermolysis of **1** in a 1:1 mixture of benzene/benzene-$d_6$ at 23 °C yields an intermolecular kinetic isotope effect of 1.04(4), a value similar to that exhibited by its tungsten congener at 70 °C.$^{36}$

**Preparation of Cp*Mo(NO)(=CHCMe$_3$)(NC$_5$H$_5$) (8).** A red solution of **1** (0.102 g, 0.253 mmol) in pyridine (8 mL) was stirred at room temperature for 30 h. The final orange-yellow solution was taken to dryness in vacuo, the remaining solid was dissolved in hexanes (10 mL), and the solution was filtered through a column of Celite (0.5 × 2 cm) supported on glass wool. The filtrate was kept at −30 °C overnight to induce the deposition of orange crystals which were collected by filtration, washed with pentane (2 × 1 mL), and dried in vacuo (0.058 g, 55% in two crops).

Anal. Calcd for C$_{20}$H$_{30}$MoN$_2$O: C, 58.53; H, 7.37; N, 6.83. Found: C, 58.39; H, 7.20; N, 6.87. $^1$H NMR (C$_6$D$_6$, 300 MHz) $\delta$ 1.60 (s, 9H, CMe$_3$), 1.79 (s, 15H, C$_5$Me$_5$), 6.18 (t, $^3J_{HH}$ = 6.9 Hz, 2H, pyridine $H_{meta}$), 6.58 (t, $^3J_{HH}$ = 7.6 Hz, 1H, pyridine $H_{para}$), 8.15 (d, $^3J_{HH}$ = 4.9 Hz, 2H, pyridine $H_{ortho}$), 12.43 (s, 1H, Mo=CH). $^{13}$C{$^1$H} NMR (C$_6$D$_6$, 75 MHz) $\delta$ 10.4 (C$_5$Me$_5$), 32.7 (CMe$_3$), 49.5 (CMe$_3$), 108.0 (C$_5$Me$_5$), 124.1 (pyridine $C_{meta}$), 136.6 (pyridine $C_{para}$), 154.8 (pyridine $C_{ortho}$), 155.0 (pyridine $C_{ortho}$), 298.4 (Mo=CH). MS (EI, 120 °C): $m/z$ 412 [P$^+$]. The NMR spectroscopic data for Cp*Mo(NO)(=CHCMe$_3$)-(NC$_5$D$_5$) (**8**-$d_5$) recorded in pyridine-$d_5$ are contained in Figure 6 and are provided below.

$^1$H NMR (pyridine-$d_5$, 500 MHz) $\delta$ 1.47 (s, 9H, CMe$_3$), 1.83 (s, 15H, C$_5$Me$_5$), 12.38 (s, 1H, Mo=CH). $^{13}$C{$^1$H} NMR (pyridine-$d_5$, 125 MHz) $\delta$ 10.4 (C$_5$Me$_5$), 32.6 (CMe$_3$), 49.5 (CMe$_3$), 108.4 (C$_5$Me$_5$), 124.6 (t, $^1J_{CD}$ = 24.5 Hz, pyridine $C_{meta}$), 137.4 (t, $^1J_{CD}$ = 25.1 Hz, pyridine $C_{para}$), 154.9 (t, $^1J_{CD}$ = 28.3 Hz, pyridine $C_{ortho}$), 298.1 (Mo=CH).

**Preparation of Cp*Mo(NO)($\eta^2$-C$_6$H$_4$)(NC$_5$H$_5$) (9).** A red solution of **6** (0.056 g, 0.136 mmol) in pyridine (5 mL) was stirred at room temperature for 24 h. The final solution was taken to dryness in vacuo, the remaining orange solid was dissolved in Et$_2$O (10 mL), and the solution was filtered through a column of Celite (0.5 × 2 cm) supported on glass wool. The filtrate was stored at −30 °C for 4 h to induce the deposition of **9** as a yellow solid. The product was isolated by decanting the orange supernatant solution (from which complex **8** can be recovered), and the yellow precipitate was washed with cold Et$_2$O (2 × 1 mL) and pentane (2 × 1 mL) and then dried in vacuo (0.010 g, 17%). Recrystallization of the yellow solid from benzene provided yellow needles of **9**·C$_6$H$_6$ suitable for analysis by X-ray diffraction. The benzyne complexes Cp*Mo(NO)($\eta^2$-C$_6$H$_4$)(NC$_5$H$_5$) (**9**) and Cp*Mo-(NO)($\eta^2$-C$_6$H$_4$)(NC$_5$D$_5$) (**9**-$d_5$) are not sufficiently soluble in C$_6$D$_6$ to characterize by $^{13}$C{$^1$H} NMR spectroscopy. Consequently their diagnostic NMR spectra were obtained with pyridine-$d_5$ solutions.

Anal. Calcd for C$_{21}$H$_{24}$MoN$_2$O: C, 60.58; H, 5.81; N, 6.73. Found: C, 60.02; H, 6.23; N, 6.36. IR (KBr): $\nu$(NO) 1537 (s) cm$^{-1}$, $\nu$(C≡C) 1583 cm$^{-1}$. $^1$H NMR (pyridine-$d_5$, 500 MHz, 25 °C) $\delta$ 1.67 (s, 15H, C$_5$Me$_5$), 7.37 (t, $^3J_{HH}$ = 6.4 Hz, 2H, pyridine $H_{meta}$), 7.48 (m, 2H, overlapping benzyne $H_{metaA}$ and $H_{metaB}$), 7.76 (t, $^3J_{HH}$ = 7.4 Hz, 1H, pyridine $H_{para}$), 7.78 (m, 1H, benzyne $H_{orthoA}$), 7.89 (m, 1H, benzyne $H_{orthoB}$), 9.02 (d, $^3J_{HH}$ = 5.1 Hz, 2H, pyridine $H_{ortho}$). $^{13}$C{$^1$H} NMR (pyridine-$d_5$, 125 MHz, 25 °C) $\delta$ 10.1 (C$_5$Me$_5$), 110.2 (C$_5$Me$_5$), 125.8

(pyridine $C_{meta}$), 127.6 (benzyne $C_{orthoB}$), 128.8 (benzyne $C_{orthoA}$), 129.1 (benzyne $C_{metaA}$), 129.5 (benzyne $C_{metaB}$), 138.6 (pyridine $C_{para}$), 156.3 (pyridine $C_{ortho}$), 158.4 (benzyne $C_{ipso}$), 162.2 (benzyne $C_{ipso}$). MS (EI, 120 °C): $m/z$ 418 [P$^+$]. The spectra of **9**-$d_5$ in pyridine-$d_5$ (e.g., Figure 6) are identical except that no pyridine signals are evident.

**Thermal Reaction of 6-$d_6$ in C$_6$D$_6$.** A glass bomb equipped with a Kontes valve was charged with a solution of **6**-$d_6$ (0.012 g, 0.029 mmol) in C$_6$D$_6$ (4 mL) and maintained at 35 °C for 48 h. A $^1$H NMR spectrum of the final solution indicated the incomplete formation of **7**-$d_{10}$ ($\delta$ 1.51) and neopentane-$d_2$ (br, $\delta$ 0.86). The proton-decoupled deuterium spectrum of the final solution was also recorded. $^2$H{$^1$H} NMR (C$_6$D$_6$, 76.8 MHz, 25 °C) $\delta$ $-1.75$ (s, C$D_{syn}$H of unreacted **6**-$d_6$), 0.86 (s, neopentane-$d_2$), 7.15 (C$_6$D$_6$), 7.57 (s, phenyl), 7.70 (s, phenyl). No deuterium signal was evident in the Cp* methyl region (ca. $\delta$ 1.5).

**Thermal Reaction of 6 in Tetramethylsilane.** Thermolysis of **6** (0.008 g, 0.020 mmol) in Me$_4$Si (5 mL) at room temperature for 48 h results in the formation of a violet solution. Evaporation of the volatile components from the final reaction mixture provided a deep red solid that was dissolved in C$_6$D$_6$. Analysis of this solution by NMR spectroscopy revealed a mixture of Cp*Mo(NO)(CH$_2$CMe$_3$)(CH$_2$SiMe$_3$) (**2**, 41%) and Cp*Mo(NO)(CH$_2$SiMe$_3$)(C$_6$H$_5$) (**10**, 59%) (product ratio determined after ca. 70% conversion). Product ratios were determined by integration of the distinctive methylene proton resonances which appear between 2.5 and 5.0 ppm. Complex **10** was not isolated but was characterized in situ by $^1$H NMR spectroscopy. $^1$H NMR (C$_6$D$_6$, 300 MHz, 25 °C) $\delta$ $-0.43$ (d, $^2J_{HH}$ = 10.7 Hz, 1H, C$H_{syn}$H), 0.23 (s, 9H, CMe$_3$), 1.49 (s, 15H, C$_5$Me$_5$), 2.79 (d, $^2J_{HH}$ = 10.7 Hz, 1H, C$H_{anti}$H), 7.09 (m, 3H, phenyl $H_{meta}$ and $H_{para}$), 7.46 (d, $^3J_{HH}$ = 6.6 Hz, 2H, phenyl $H_{ortho}$).

**Thermal Reaction of 6 in PMe$_3$.** Thermolysis of **6** (0.049 g, 0.122 mmol) in PMe$_3$ (1 mL) at room temperature for 24 h resulted in the formation of a brown solution containing Cp*Mo(NO)(=CHCMe$_3$)-(PMe$_3$). This complex was not isolated but was characterized by a $^1$H NMR spectrum of the dried reaction residue in C$_6$D$_6$. $^1$H NMR (C$_6$D$_6$, 300 MHz, 25 °C) $\delta$ 0.95 (d, $^2J_{HP}$ = 8.5 Hz, 9H, PMe$_3$), 1.40 (s, 9H, CMe$_3$), 1.84 (s, 15H, C$_5$Me$_5$), 12.38 (d, $^3J_{HP}$ = 4.4 Hz, 1H, Mo=C$H$).

**X-ray Crystallographic Analyses.** Data collection and structure solution for Cp*Mo(NO)(CH$_2$CMe$_3$)$_2$ (**1**) and Cp*Mo(NO)(=CHCMe$_3$)-(NC$_5$H$_5$) (**8**) were conducted at the University of Southern California. X-ray data were collected at low temperature (130(2) K for **1** and 160-(5) K for **8**) on a Bruker SMART APEX CCD diffractometer with graphite-monochromated Mo K$\alpha$ radiation ($\lambda$ = 0.710 73 Å). The cell parameters for each compound were obtained from the least-squares refinement of the spots (from 60 collected frames) using the SMART program.[40] In each case, a hemisphere of data was collected up to a resolution of 0.75 Å, and the intensity data were processed using the SAINT PLUS program.[41] All calculations for the structural analyses were carried out using the SHELXTL package.[42] Initial positions of the Mo atoms were located by direct methods, and the rest of the atoms were found by using conventional heavy-atom techniques. The structures were ultimately refined by least-squares methods using data in the range of 2$\theta$ = 3.5−55.0°.

For the complex Cp*Mo(NO)(CH$_2$CMe$_3$)$_2$ (**1**), all hydrogen atoms were placed in calculated positions except the four H atoms of the two CH$_2$ groups. Those were readily located from difference Fourier maps and were subsequently refined isotropically. The structure of **1** is remarkably similar to that of the analogous tungsten complex, Cp*W-(NO)(CH$_2$CMe$_3$)$_2$.[8] As in the case of the tungsten analogue, one of the neopentyl groups in **1** has disordered methyl groups, but fortunately, the methylene portion of this CH$_2$CMe$_3$ ligand was ordered, and its two H atoms could be located unambiguously. For the complex Cp*Mo-

(NO)(=CHCMe$_3$)(NC$_5$H$_5$) (**8**), basically the same strategy was followed. The position of the unique methine hydrogen was located from a difference Fourier map while all other hydrogens were placed in calculated positions. In the subsequent least-squares refinement, all non-hydrogen atoms were refined anisotropically, and all hydrogens were refined isotropically in a riding manner along with their attached carbons except the unique hydrogen of the =CH group which was allowed to refine independently. The final position of that H atom corresponds to a normal sp$^2$-hybridized carbon atom with very little hint of an Mo··· ·H agostic interaction.

Data collection and structure solution for Cp*Mo(NO)(CH$_2$CMe$_3$)-($\eta^2$-CH$_2$C$_6$H$_3$-3,5-Me$_2$) (**3**), Cp*Mo(NO)(CH$_2$CMe$_3$)(C$_6$H$_5$) (**6**), and Cp*Mo(NO)($\eta^2$-C$_6$H$_4$)(NC$_5$H$_5$)·C$_6$H$_6$ (**9**·C$_6$H$_6$) were conducted at the University of British Columbia. All measurements were recorded at $-100(1)$ °C on a Rigaku/ADSC CCD area detector using graphite-monochromated Mo K$\alpha$ radiation. For **3**, the data were collected to a maximum 2$\theta$ value of 55.8° in 0.50° oscillations with 12.0 s exposures. A sweep of data was done using $\phi$ oscillations from 0.0 to 190.0° at $\chi$ = $-90.0°$, and a second sweep was performed using $\omega$ oscillations between $-17.0°$ and 23.0° at $\chi$ = $-90°$. The crystal-to-detector distance was 38.19 mm, and the detector swing angle was $-5.58°$. For **6**, the data were collected to a maximum 2$\theta$ value of 55.8° in 0.50° oscillations with 20.0 s exposures. A sweep of data was done using $\phi$ oscillations from 0.0 to 190.0° at $\chi$ = $-90.0°$, and a second sweep was performed using $\omega$ oscillations between $-17.0°$ and 23.0° at $\chi$ = $-90°$. The crystal-to-detector distance was 38.14 mm, and the detector swing angle was $-5.60°$. For **9**·C$_6$H$_6$, the data were collected to a maximum 2$\theta$ value of 55.7° in 0.50° oscillations with 57.0 s exposures. A sweep of data was done using $\phi$ oscillations from 0.0° to 190.0° at $\chi$ = $-90.0°$, and a second sweep was performed using $\omega$ oscillations between $-17.0°$ and 23.0° at $\chi$ = $-90°$. The crystal-to-detector distance was 37.99 mm, and the detector swing angle was $-5.60°$. All three data sets were corrected for Lorentz and polarization effects. The solid-state structures were solved by direct methods[43] and expanded using Fourier techniques.[44] The non-hydrogen atoms were refined anisotropically. For **3**, only the methylene hydrogens on C(11) and C(20) were refined isotropically. For **6**, the phenyl hydrogens and the methylene hydrogens on C(17) were refined isotropically. All other hydrogen atoms in **3**, **6**, and **9**·C$_6$H$_6$ were placed in calculated positions. The final cycles of full-matrix least-squares refinements (function minimized, $\Sigma w(F_o^2 - F_c^2)^2$) were based on 5058 observed reflections and 270 variable parameters for **3**, 4610 observed reflections and 253 variable parameters for **6**, and 5081 observed reflections and 285 variable parameters for **9**·C$_6$H$_6$. All calculations were performed using the *teXsan* crystallographic software package of Molecular Structure Corporation[45] and SHELXL-97.[42] Selected crystallographic data for the X-ray structures of **1**, **3**, **6**, **8**, and **9**·C$_6$H$_6$ are presented in Table 1. Full details of all crystallographic analyses are provided as Supporting Information.

**Kinetic Studies.** Kinetic studies of the reaction of **1** in C$_6$D$_6$ were performed using a J. Young NMR tube containing a solution of **1** (12 mg, 0.03 mmol) in 1 mL of C$_6$D$_6$ with a fused capillary tube containing hexamethyldisilane as an internal standard. The reaction was conducted in the NMR probe at constant temperature, and $^1$H NMR spectra were recorded at intervals. The rate constants were calculated using linear regression methods from first-order plots of the loss of starting material versus time.

**Theoretical DFT Calculations.** To compare the single-point energies of model complexes in a consistent manner, all calculations were carried out using geometries optimized by density functional theory

(40) *SMART APEX program system*, version 5.0; Bruker Analytical X-ray System, Inc.: Madison, WI, 2001.
(41) *SAINT PLUS program system*, version 5.0; Bruker Analytical X-ray System, Inc.: Madison, WI, 2001.
(42) Sheldrick, G. M. *SHELXTL*, version 5.1; Bruker Analytical X-ray System, Inc.: Madison, WI, 1997.
(43) For SIR97, see: Altomare, A.; Burla, M. C.; Cammalli, G.; Cascarano, M.; Giacovazzo, C.; Guagliardi, A.; Moliterni, A. G. G.; Polidori, G.; Spagna, A. *J. Appl. Crystallogr.* **1999**, *32*, 115−119.
(44) *DIRDIF-94 program system*; Technical Report of the Crystallography Laboratory; University of Nijmegen: The Netherlands, 1994.
(45) *teXsan*, Crystal Structure Analysis Package; Molecular Structure Corporation: 3200 Research Forest Drive, The Woodlands, TX, 77381, 1985 and 1992.

(DFT). Calculations were performed using the Gaussian 98 RevA.11.1[46] implementation of B3LYP (Becke three-parameter exchange functional (B3)[47] and the Lee−Yang−Parr correlation functional (LYP)[48]) in the parallel execution environment using the Scientific Computing Associates' Linda program suite on the Fujitsu VPP-800 supercomputer at the Academic Center for Computing and Media Studies, Kyoto University. A part of the computations was performed on Intel PII computers at the University of British Columbia. Four basis sets were considered. Most of the calculations utilized the LanL2DZ basis set that included D95 basis functions for H, C, N, and O[49] and the relativistic electron core potential (ECP) sets of Hay and Wadt for Mo.[50] In this connection, it should be noted that the alkylidene fragment CpMo(NO)(=CH$_2$) **D**, the $\sigma$-methane complex CpMo(NO)(=CH$_2$)($\sigma$-CH$_4$) **C**, the dimethyl complex CpMo(NO)(CH$_3$)$_2$ **A**, and the transition-state species CpMo(NO)(=CH$_2$···H···CH$_3$) **B-TS** have previously been optimized by Poli and Smith.[35] The second basis set, designated SDD, was the combination of the Huzinage−Dunning double-$\zeta$ basis set on lighter elements with the Stuttgart−Dresden basis set−RECP combination.[51] The third basis set, LanL2DZ-II, combined the D95* basis functions on the lighter elements with LanL2DZ on the molybdenum

atom, supplemented by $f$-type polarization functions taken from the work of Frenking and co-workers.[52] In the fourth basis set, LanL2DZ-III, the modified ECP in which the two outermost $p$ functions were replaced by a (41) split of the optimized $5p$ function[53] was employed for the Mo atoms together with the 6-31G* basis set for all C, N, and O atoms, the 6-31G** basis set for all H atoms on CH$_3$ and C$_6$H$_5$ groups, and the 6-31G basis set for all cyclopentadienyl H atoms. No constraints were imposed on any of the systems. Frequency calculations on optimized species established that all the transition states possessed only one imaginary frequency and that the products and intermediates possessed no imaginary frequencies. Energies with thermal corrections ($E$) and Gibbs free energies ($G$) were computed for species in the gas phase at standard temperature (298.15 K) and pressure (1 atm). Spatial plots of the optimized geometries and frontier orbitals were obtained from Gaussian 98 output using Cambridge Soft Corporation's Chem 3D Pro v4.0.

**Supporting Information Available:** Full details of crystallographic (CIF) and theoretical (PDF) analyses. This material is available free of charge via the Internet at http://pubs.acs.org.

JA0349094

(46) Frisch, M. J.; Trucks, G. W.; Schlegel, H. B.; Scuseria, G. E.; Robb, M. A.; Cheeseman, J. R.; Zakrzewski, V. G.; Montgomery, J. A., Jr.; Stratmann, R. E.; Burant, J. C.; Dapprich, S.; Millam, J. M.; Daniels, A. D.; Kudin, K. N.; Strain, M. C.; Farkas, O.; Tomasi, J.; Barone, V.; Cossi, M.; Cammi, R.; Mennucci, B.; Pomelli, C.; Adamo, C.; Clifford, S.; Ochterski, J.; Petersson, G. A.; Ayala, P. Y.; Cui, Q.; Morokuma, K.; Malick, D. K.; Rabuck, A. D.; Raghavachari, K.; Foresman, J. B.; Cioslowski, J.; Ortiz, J. V.; Stefanov, B. B.; Liu, G.; Liashenko, A.; Piskorz, P.; Komaromi, I.; Gomperts, R.; Martin, R. L.; Fox, D. J.; Keith, T.; Al-Laham, M. A.; Peng, C. Y.; Nanayakkara, A.; Gonzalez, C.; Challacombe, M.; Gill, P. M. W.; Johnson, B. G.; Chen, W.; Wong, M. W.; Andres, J. L.; Head-Gordon, M.; Replogle, E. S.; Pople, J. A. *Gaussian 98*, revision A.11.1; Gaussian, Inc.: Pittsburgh, PA, 1998.
(47) Becke, A. D. *J. Chem. Phys.* **1993**, *98*, 5648−5652.
(48) Lee, C.; Yang, W.; Parr, R. G. *Phys. Rev.* **1988**, *B37*, 785−789.
(49) Dunning, T. H. J.; Hay, P. J. In *Modern Theoretical Chemistry*; Schaefer, H. F., III, Ed.; Plenum Press: New York, 1976; pp 1−28.
(50) (a) Hay, P. J.; Wadt, W. R. *J. Chem. Phys.* **1985**, *82*, 270−283. (b) Wadt, W. R.; Hay, P. J. *J. Chem. Phys.* **1985**, *82*, 284−298. (c) Hay, P. J.; Wadt, W. R. *J. Chem. Phys.* **1985**, *82*, 299−310.
(51) Dolg, M. In *Modern Methods and Algorithms of Quantum Chemistry*; Grotendorst, J., Ed.; John van Neumann Institute for Computing: Zürich, 2000; Vol. 1, pp 479−508.
(52) Ehlers, A. W.; Böhme, M.; Dapprich, S.; Gobbi, A.; Höllwarth, A.; Jonas, V.; Köhler, K. F.; Stegmann, R.; Veldkamp, A.; Frenking, G. *Chem. Phys. Lett.* **1993**, *208*, 111−114.
(53) Couty, M.; Hall, M. B. *J. Comput. Chem.* **1996**, *17*, 1359−1370.